The *In Vitro* Delivery of Doxorubicin using Biosynthesized versus Chemically Synthesized Stealth Site-Specific Bimetallic Selenium-Silver Nanoparticles

Submitted in partial fulfilment for the Master of Applied Science (Biotechnology) in the Department of Biotechnology and Food Science, Durban University of Technology, Durban, South Africa

Thoko Winnie Malinga
Student Number: 21737644

2021-2022

PROMOTER/ SUPERVISOR	**: Prof. Tukayi Kudanga**
CO-PROMOTER/ CO-SUPERVISOR	**: Dr. Londiwe Simphiwe Mbatha**

DECLARATION

I hereby declare that the work reported in this dissertation and submitted to the Department of Biotechnology and Food Science at Durban University of Technology for a Masters degree is my original work. I confirm that it has not been previously submitted for a degree at any Higher Education Learning Institution.

09/04/2023

Thoko Winnie Malinga **Date**

Student

As the candidate's supervisors we agree to the submission of this thesis

09/04/2023

Prof Tukayi Kudanga

Date

Supervisor

09/04/2023

Dr Londiwe Simphiwe Mbatha **Date**

Co-Supervisor

ABSTRACT

Problems related to the limitations of chemotherapeutic treatments compel the pressing necessity to develop a drug-delivery system that will specifically target tumor cells and have minimal or no harmful effects on normal/healthy cells. This study aimed to comparatively evaluate the ability of chemically versus biologically synthesized site-specific selenium-silver bimetallic stabilized folic targeted nanoparticles (SeAgChPEGFA NPs) to efficiently deliver doxorubicin (DOX) in cervical cancer cells (HeLa). The NPs were synthesized using a co-reduction method chemically using sodium borohydride and polyvinylpyrrolidone, and biologically using fenugreek seed extract. Moreover, the NPs from both methods of synthesis were stabilized and functionalized using carbodiimide and adsorptionreaction procedures. The drug/DOX-loaded nanocomplexes (NCs) were prepared via anadsorption and amide bonding reaction process between the co-polymer stabilized NPs and DOX. The bimetallic NPs and their DOX-loaded NCs were characterized using ultraviolet- visible (UV-vis) spectroscopy, Fourier-transform infrared spectroscopy (FTIR), transmission electron microscopy (TEM), and *zeta* Sizer. The drug release, loading, and encapsulation capabilities were evaluated in an *in vitro* environment. The effects of the synthesized NCs on cell viability and programmed cell death analysis were evaluated by means of the 3-(4,5-Dimethylthiazol-2-yl)-2,5-diphenyltetrazolium bromide (MTT) assay and a dual staining technique in selected human non-cancer and cancer cell lines (HEK293 and HeLa cells), respectively.

The NPs and their drug-loaded NCs were successfully formulated and characterized. The successful synthesis of the NPs was initially validated by the reaction mixtures' change in colour from cloudy to red-orange and subsequently from yellow-gold to orange-brown, signifying the formation of SeAg NPs and F-SeAg NPs, respectively. The UV- spectroscopy revealed that the SeAg NPs absorbance peaks were between 260 nm and 320 nm, while the FTIR verified the stabilization and functionalization of the NPs by revealing the presence of carbodiimide and amide bonds. All the resultant NPs and their drug-loaded NCs were shown as spherical withthe NPs appearing predominantly monodispersed and the NCs as groups. The sizes of the chemically and biosynthesized NPs ranged between 103.5 nm and 138.8 nm and that of the DOX-loaded NCs ranged between 154.9 nm and 158.7 nm respectively. The DOX-loaded chemically- and biologically-synthesized NCs showed good stability with *zeta* measurements of 53.1 ± 2.3 mV and 57.4 ± 1.9 mV, respectively. The encapsulation efficiency (EE%) and drug loading (DL%) percentages of the chemically synthesized NCs were calculated to be 84% and 26%, respectively, while the percentages of the biosynthesized NCs were 87% and 22%, respectively. The cytotoxicity and anticancer activities of the BMNPs/NCs from both methods of synthesis were cell-specific and concentration-dependent.

Overall, the encapsulation of DOX to the eco-friendly formulated BNPs enhanced the biocompatibility, bioavailability, and therapeutic effects of the drug in tumor cells, with limited harm to the healthy cells, thus showing promise as alternative delivery systems for targeted

cancer treatment. The findings indicated that both the chemically synthesized and biosynthesized NPs showed great potential as anticancer drug-delivery modalities, with the biosynthesized SeAgChPEGFA@DOX NCs showing superior optical, surface charge stability, and drug encapsulation properties than the chemically synthesized SeAgChPEGFA@DOX NCs and free DOX. Moreover, among the studied synthesis methods, biosynthesis is reported to be eco-friendly and as a result the more ideal anticancer drug-delivery system with favourable features for future *in vivo* applications. Thus, future studies can encompass *in vivo* assessment of this eco-friendly system to further evaluate at a broader scale the bimetallic system's efficacy and safety before using these NPs clinically.

TABLE OF CONTENTS

LIST OF FIGURES

LIST OF TABLES

LIST OF ABBREVIATIONS

Abbreviation	Definition
µg	Microgram
µl	Microliter
A549	Lung cancer cells
Ag	Silver
AI	Apoptotic index/indices
AO	Acridine orange dye
Apaf-1	Apoptotic protease factor -1
Au	Gold
B.C	Before Christ
BMNPs	Bimetallic nanoparticles
CCM	Colloidal crystal mask
Ca2+	Cellular calcium
Ch	Chitosan
CPT	Camptothecin
Cyt-c	Cytochrome-c
DCCI	N'- dicyclohexyl-carbodiimide
DL%	Drug loading percentage
DMSO	Dimethyl sulphoxide
DNA	Deoxyribonucleic acid
DOX	Doxorubicin
EA	Early apoptosis
EDC	1-(3- dimethylaminopropyl)-3-ethylcarbodiimide
EE%	Encapsulation efficiency percentage
EMEM	Eagle's Minimum Essential Medium
ER	Endoplasmic reticulum
EtBr	Ethidium bromide dye
F	Fenugreek seed extract
FA	Folic acid
FA-Rs	Folic acid receptors
FBS	Fetal bovine serum
FDA	Food and Drug Administration
FTIR	Fourier-transform infrared spectroscopy
HEK293	Human embryonic kidney cells
HeLa/ SiHa	Human cervical cancer cells
HepG2	Human hepatoma/ liver cancer cells
HUVECs	Human umbilical vein endothelialcells
IC_{50}	Half maximal inhibitory concentration
L	Live cells
LA	Late apoptosis
LSPR	Localized surface plasmon resonance

MAPK/Erk	Mitogen-activated protein kinase/extracellular-signal-regulated kinase
MC3T3	Normal pre-osteoblast cell line
mg	Milligram
ml	Milliliter
mM	Millimolar
MNPs	Metal/metallic nanoparticles
Mt	Mitochondria/Mitochondrial
mTOR	Mammalian target of rapamycin
MTT	3-(4,5-Dimethylthiazol-2-yl)-2,5- diphenyltetrazolium bromide
NADPH	Nicotinamide adenine dinucleotide phosphate
NCs	Nanocomplexes
NFκB	Nuclear factorkappa B
NHS	N'-hydroxysuccinimide
NLS	Nanosphere lithography
NPs	Nanoparticles
PARP-1	Poly ADP-ribose Polymerase-1
PBS	Phosphate buffer saline
PEG	Polyethylene glycol
PEI	Poly (ethyleneimine)
PI3K/Akt	Phosphatidylinositol-3-kinase
PLG	Poly(d,l-lactide-co-glycolide)
PLL	Poly(L-lysine)
PP	Peach plant leaf extract
Pt	Platinum
PVP	Polyvinylpyrrolidone
RIPK3	Receptor-interacting serine/threonine-protein kinase 3
RNA	Ribonucleic acid
ROS	Reactive oxygen species
rpm	Revolutions per minute
SD	Standard deviation
Se	Selenium
SeAg NPs	Selenium silver nanoparticles
SeAgChPEG NPs	Selenium silver chitosan pegylated nanoparticles
SeAgChPEGFA NPs	Selenium silver chitosan pegylated folate targeted nanoparticles
SeAgChPEGFA@DOX NCs	Selenium silver chitosan pegylated folate targeted doxorubicin conjugated nanocomplexes
TEM	Transmission electron microscopy
Ti	Titanium
UV-vis	Ultra violet visible

ACKNOWLEDGEMENTS

I would like to express my utmost gratitude and appreciation to:

- The higher being for giving me strength, patience, and wisdom to carry out my studies through all the obstacles I have encountered.

- My supervisor Prof. T Kudanga and co-supervisor Dr. L.S Mbatha for allowing me to work on such a big project, for their guidance throughout the investigation,and for all the advice on how to better my research skills.

- The University of KwaZulu Natal for allowing me to use its research facilities.

- The Durban University of Technology and the National Research Foundation for financially supporting my research project.

- My family and friends for their building words of support and encouragement, which made me more eager to complete this research project and thesis.

This thesis is dedicated to my parents Dumisani Hendrick and Jessie Nomangisi Malinga, and brothers Thokozani, Mthokozisi, and Mthobisi Malinga for their endless love, support, and encouragement throughout these years.

I. Chapter One: Introduction

1.1 Background and Research Problem

Cancer has remained the leading cause of mortality, accounting for approximately 10 million deaths across the globe in 2020 (Okugawa *et al.*, 2021). Amongst the different kinds of cancers reported, cervical cancer has been identified as one kind that has been increasing significantly all over the globe (Carlson *et al.*, 2012; Al Rifai and Nakamura, 2015), contributing to over 300000 deaths in 2020, despite available treatments (Sung *et al.*, 2021).

There are a few methods to treat cancer that are in place. These include surgery, radiation/radiotherapy, hormone therapy, chemotherapy, and their combinatorial treatments. However, these treatments are associated with several limitations, including non-specificity, toxicity, fast clearance, limited bioavailability, and may exhibit low efficiency instopping metastasis (Vaid *et al.,* 2020). Amongst these treatments, chemotherapy has been a hallmark of treating cancers (Peter *et al.,* 2022). This technique involves the direct administration of synthetic drugs such as doxorubicin, 5-fluorouracil, cisplatin, fludarabine, ibandronic acid, and raloxifene in cancer patients. Amongst these drugs, doxorubicin has been used in numerous cancer studies due to its effectiveness in treating several types of cancer (Peter *et al.,* 2022). The drugs function through even biodistribution throughout the body, preventing the division of abnormal cells by intervening in the cellular activities that are essential for their division. Yet, these antineoplastic drugs lack the ability to differentiate normal cells from cancer cells, and they reach most normal cells as well as tumor cells/tissues by free diffusion, resulting in systemic toxicity. This limits their clinical use at increased doses which leads to some severe side effects such as cardiotoxicity, renal toxicity, and gonadotoxicity. In addition, the intravenous/oral administration of chemotherapeutic drugs yields a low therapeutic effect due to the biodegradation of the drugs by enzymes in biological systems. Thus, there is still a need to develop drug-delivery systems that are safe, can protect drugs from degradation upon administration, and specifically deliver the drugs to the target sites, thereby enhancing efficacy whilst reducing toxic effects on normal cells.

Nanomedicine presents an alternative solution to this ongoing problem, by proposing the application of nanoparticles (NPs), particularly, metal NPs as drug carrier vectors. They can be formulated through nanotechnology techniques, categorized as physical, chemical, or biological/green methods (Dang and Guan, 2020). Amongst these methods, the chemical and green synthesis methods have been studied in depth because they are easy to use and the yield, toxicity and stability of the NPs can be controlled during formulation (Ijaz *et al.*, 2020). However, the biological synthesis of NPs is deemed safer than chemical synthesis because it does not utilize any harsh chemicals in any of its formulations (Dang and Guan, 2020). During chemical synthesis, chemicals such as sodium borohydride, ascorbic acid, hydrazine, and hydrogen are commonly used to reduce metalions into metal NPs (Khandel *et al.,* 2018). While during biosynthesis, natural agents suchas plant extracts (e.g., seeds or leaves extracts) and microorganisms like bacteria, fungi, and algae are used to reduce metal ions into metal NPs. The application of these methods allows a vast variety of NPs formulations, including but not limited to metal NPs such as titanium (Ti), platinum (Pt), gold (Au), silver (Ag), and selenium (Se), with unique features such as exceptional physicochemical stability, large surface to volume ratio, photocatalytic and optical properties to be used in cancer therapy. The desirable properties allow them to efficiently bind, absorb, carry, and deliver anticancer drugs to the desired sites. Over the years, various studies have been reported on these metal NPs as anticancer drug carriers (Alshatwi et al., 2015; Cordani and Somoza, 2019; Huy et al., 2020).

Recently, bimetallic NPs are attracting more interest than monometallic NPs due to their synergistic characteristics, such as enhanced catalytic properties, considering that bimetallization improves the original mono-metal catalyst's properties by creating combined new properties (Dang and Guan, 2020; Atta *et al.,* 2021). However, limited studies have been reported, hence much research is still needed to explore these bimetallic NPs. Therefore, in the current study, bimetallic Se-Ag NPs were chemically and biologically synthesized, functionalized, and evaluated for their ability to deliver an anticancer drug safely and efficiently to the selected cancer cell lines. Selenium is a vital

micronutrient acquired from dietary sources and is documented to encompass anticancer, antioxidant, antibacterial, and antibiofilm properties (Maiyo and Singh, 2017). Its nano forms (Se NPs) have attracted significant attention as potential novel drug delivery entities possessing additional photoelectric properties and high photoconductivity (Vahdati and Moghadam, 2020).

Furthermore, Ag NPs are extensively known for their high electrical and thermal conductivity in addition to their medical and therapeutic benefits, which include antifungal, anti-inflammatory, antiviral, and antiplatelet properties (Beyene *et al.,* 2017). These NPs possess other attractive characteristics, such as ease of synthesis, tenable stability, reduced cytotoxicity, exceptional biodegradability, biocompatibility, drug loading capacity, and docility to synthetic modification (Senapati *et al.*, 2018). The amenability to synthetic modification allows for surface stabilization and functionalization, which is needed for the effective biological application of the NPs as drug-delivery systems. This is usually achieved through passive targeting (modifying NPs' surface with polymers/co-polymers) and active targeting (modification of NPs' surface with specific agents or moieties) (Sohn *et al.*, 2017).

Substances such as chitosan (Ch), polyethylene glycol (PEG), and folic acid (FA) have been successfully utilized to fine-tune NPs for biological applications (Park *et al.*, 2017; Gulati *et al.,* 2018) and for that reason they were selected for the stabilization and functionalization of the synthesized bimetallic Se-Ag NPs in this study. Ch is a positively charged amphiphilic polysaccharide with high bio-adhesiveness, low cytotoxicity, and high buffering capacity (Collado-González *et al.,* 2017). The positively charged Ch binds and protects the drug from degradation by intracellular enzymes. It also facilitates the binding of the drug-loaded NPs to the surface of cells and subsequent cellular uptake and facilitates the intracellular release of the therapeutic drug due to its high buffering capacity (Richard *et al.,* 2013; Parhi, 2020; Aibani *et al.,* 2021; Frigaard *et al.,* 2022). PEG on the other hand is a hydrophilic polyether that shields NPs from inactivation by the immune system. It is widely used as a gold standard in bio-conjugation and nanomedicine due to its ability to prolong the blood circulation period of the NPs or drug-loaded NPs

resulting in the improvement of therapeutic efficacy (Shariatinia, 2019; Frank *et al.,* 2020). PEG is also biodegradable, biocompatible, and has low cytotoxicity. Herein, these polymers have been chosen to work synergistically as they have been reported to have the appropriate biological properties to be used in pharmaceutical applications. Furthermore, to increase target precision, a folate targeting agent was conjugated onto the NPs. Most cancer cells have been reported to overly express folate receptors on their outermost membrane and as a result, FA is frequently used as a targeting agent due to its high affinity to the folate receptors. Additionally, FA is non-toxic, biodegradable, and biocompatible (Leamon *et al.*, 2014; Scaranti *et al.*, 2020). The chosen bio substances cover all the limiting aspects currently faced by the currently used chemotherapy to produce an improved and safe alternative.

1.2 Aim

- To evaluate and compare the ability of site-specific chemically synthesized versus biologically synthesized bimetallic SeAgChPEGFA nanoparticles to efficiently deliver doxorubicin in cervical cancer cells.

1.3 Objectives

- To synthesize (chemically and biologically) and confirm the synthesis of the SeAgNPs/SeAgChPEGFA and their DOX-loaded nanocomplexes (NCs).
- To determine the ultrastructural morphology, size, *zeta* potential, and dispersity of the synthesized NPs/DOX-loaded NCs.
- To evaluate the *in vitro* release profiles, drug loading, and encapsulation efficiency of the DOX-loaded NCs.
- To evaluate the cytotoxicity and anticancer profiles of the synthesized NPs and their DOX-loaded NCs in cervical cancer.

1.4 Outline of Thesis

The thesis is structured with chapters 1-5 as presented:

- **Chapter One:** A brief introduction to the current study's background, problem statement, novelty, aims, and objectives.
- **Chapter Two:** An in-depth literature review on the research topic.
- **Chapter Three:** Experimental details including the materials and methods used to formulate, characterize and evaluate the novel selenium-silver nanoparticles and nanocomplexes.
- **Chapter Four:** Results and Discussion.
- **Chapter Five:** General Discussion, Conclusion, and Recommendations.

II. Chapter Two: Literature Review

2.1 Introduction

Cancer is an illness that results from genetic or epigenetic mutations in the somatic cells which cause uncontrolled cell proliferation at a specific site in the body that can spreadto other sites (Saini *et al.,* 2020; ul Hussain *et al.*, 2022). These abnormally proliferating cells lead to the formation of tumors represented as lumps or masses of tissue. Tumors are classified into cancerous (malignant tumors) and non-cancerous (benign tumors) depending on their ability to metastasize (Saini *et al.,* 2020). The malignant tumors can grow on tissues near their primary location and mobilize to distant regions in the body to form new tumors through metastasis. Benign tumors remain in their primary location without invading or spreading to other distant sites of the body (Patel, 2020).

There are different types of cancer, which are classified based on their region of origin and the type of cell they are made of (Liu, 2003). These types include but are not limited to carcinomas, sarcomas, leukemias, lymphomas, central nervous system cancers, multiple myeloma, and melanoma (Saini *et al.,* 2020). This study focuses its examination on a carcinoma called cervical cancer. This type of cancer represents a serious health issue as the fourth most frequently diagnosed cancer in women living in developing countries (commonly diagnosed in 28 countries and the leading cause of mortality in 42 countries) despite available treatments (Gurram *et al.,* 2020; Okugawa *et al.*, 2021). Current treatments in place to fight cervical cancer include surgery, radiotherapy, chemotherapy, or a combination of these techniques (Maiyo and Singh, 2019); and theseare discussed in detail below.

2.1.1 Surgery

Cancer surgery is generally a procedure used to cut out a tumor and possibly some of the nearby tissues (Ramirez *et al.,* 2014). It is often used as a debulking or primary measure of tumor removal depending on the size of the tumor, its stage, and future fatality possibilities (Davenport *et al.,* 2015; Sharma *et al.*, 2019). Upon diagnosis of the size and stage of the tumor, the patient is taken to an operating theatre, gets sedated, and the

surgeon makes an incision. In the case of cervical cancer, the tumor can be removed either by cutting away the tumor only, removing the cervix (trachelectomy) or removing the cervixand uterus (hysterectomy) (Ramirez *et al.,* 2014). Though this treatment eases the pain or discomfort caused by a tumor pressing on bone nerves, its disadvantages include prolonged pain at the surgery site, negative reactions to the drugs used to numb the pain (local anesthesia), infections at the site, damage to nearby tissues, internal bleeding, slow recovery, and high chances of tumor reemergence.

2.1.2 Radiation Therapy

Radio/radiation therapy uses high-powered energy rays referred to as ionizing radiation to kill cancer cells or cause genetic changes resulting in cancer cell death through the formation of ions (particles with an electric charge) and the deposition of energy in the cells of the tissues it passes through (Baskar *et al.,* 2012). This can either be accomplished through external beam radiation therapy by leading the beams of radiation to theaffected site of the body or internally by means of positioning a radioactive material- loaded device inside the affected area (e.g., inside the vaginal area for cervical cancer therapy), usually for only a few minutes (brachytherapy) or by combining the administration techniques (Baskar *et al.,* 2012). Radiation therapy can also be used in combination with chemotherapy as the primary treatment for locally advanced cervical cancers (Tannock, 1989) and following surgery, if there is an increased risk of relapse (Thariat *et al.,* 2013). The advantages of this technique include its abilityto lower the risk of local recurrence and distant metastases; its cons include its possible cause of excessive nausea, hair loss, and swelling (termed lymphedema).

2.1.3 Chemotherapy

Chemotherapy involves the use of Food and Drug Administration (FDA) approved anticancer agents (e.g., doxorubicin, docetaxel, tamoxifen) which inhibit cancer cell proliferation and tumor multiplication (Chu and Sartorelli, 2018). The chemotherapeutic agents/drugs can be administered intravenously using an injection or orally in the form of pills/capsulated anticancer drugs. These administration techniques are used as neoadjuvant (before primary treatment), adjuvant (in addition to initial therapy), or in

combination with other cancer treatments (Chu and Sartorelli, 2018). Upon administration, the drugs widely travel throughout the body damaging the ribonucleic acid (RNA) or deoxyribonucleic acid (DNA). Subsequently, the occurrence instructs the cells how to replicate themselves during cell division, ultimately leading to programmed death of the affected cells, thus avoiding invasion and metastasis (Chu and Sartorelli, 2018). Due to this ability, this technique is considered to play the most vital role compared to the other treatments, given that surgery and radiation function to merely treat a specific area (Menon *et al.*, 2018). Chemotherapy functions by reaching tumors in different sites of the body, some of its drawbacks include excessive nausea, hair loss, fatigue, and non-specificity. These are detrimental to healthy/normal cells, and susceptible to infections due to low blood cellcounts.

Overall, the common limitation faced by the above-discussed treatments is their inability to eradicate cancer cells safely and completely, eventually leading to cancer regrowth. That said, the limitations/disadvantages of these treatments necessitate the improvement of cancer treatments. Therefore, innovations in coupling nanotechnology with biotechnology have emerged to improve the existing drug-delivery systems.

2.2 Nanotechnology and Nanoparticles

In the last few years, nanotechnologies coupled with biotechnology have transformed chemotherapeutic cancer therapy and diagnosis, employing nanomaterial-mediated drug-delivery systems (Park *et al.*, 2017; Maiyo and Singh, 2017; Maiyo and Singh, 2019). Nanotechnology involves the use of nanostructures called nanoparticles (NPs) engineered and manufactured by manipulating various materials on an atomic and molecular scale. These NPs have unique optical and electrical properties, tunable size, rich surface charge, and large surface-area-to-volume ratio, which enables them to carry anticancer agents, such as drugs, deoxyribonucleic acid (DNA), ribonucleic acid (RNA), and proteins, along with other biocompatible agents, with high efficiency (Rizvi and Saleh, 2018; Senapati *et al.*, 2018). Examples of NPs include but are not limited to micelle, dendrimer, liposome, and metallic NPs. Amongst these, metallic NPs have gained more attention as drug-

delivery systems in cancer studies, which can be attributed to the unique properties these NPs possess. These include optical properties such as low toxicity, high biocompatibility, biodegradability, tunable stability, and amenability to synthetic modification (Burdușel *et al.*, 2018; Ivanova *et al.*, 2018).

Over the last few decades, selenium (Se) and silver (Ag) NPs have been individually studied immensely due to their desired activities as metallic NPs, including antioxidant, anticancer, catalytic, and antibacterial activities (Ivanova *et al.*, 2018; Olawale *et al.,* 2021). Selenium is an important micronutrient obtained from dietary sources. It displays distinctive activity in preventing the manifestation of cancer, decreasing the toxicity of drugs, regulating thyroid gland functioning, and ensuring exceptional immune system functioning, therefore playing a huge role in fighting diseases (Jabłońskaand Reszka, 2017; Maiyo and Singh, 2017; Liu *et al.*, 2021). The nanoforms of Se (Se NPs)have been identified for usage as conventional anticancer drug delivery systems. Various studies suggest that Se has the potential to decrease systemic toxicities related to conventional antineoplastic drugs, while working synergistically to enhance efficacy. Some properties that make Se an appealing drug carrier include low toxicity, high bioavailability, and biocompatibility to name a few (Maiyo and Singh, 2017; Alam *et al.*, 2019; Fardsadegh and Jafarizadeh-Malmiri, 2019). Silver, on the other hand, is a transitionmetal that occurs as a lustrous white element and possesses high electrical and thermal conductivity (Beyene *et al.,* 2017; Alwhibi *et al.*, 2018; Burdușel *et al.*, 2018). The nano forms of Ag (Ag NPs) have gained a lot of interest in therapeutic applications attributable to their enhanced properties (Hembram *et al.*, 2018; Huy *et al.*, 2020). These properties include but are not limited to, biocompatibility, biodegradability, tunable stability, and inertness. In addition, Ag NPs possess high antimicrobial activity, anticancer activity and the capacity to be easily synthesized chemically and biologically (biosynthesis) using various microorganisms and plant extracts, hence they have been the subject of research and well-documented for years (Alwhibi *et al.*, 2018; Burdușel *et al.*, 2018; Olawale *et al.,*2021).

2.3 Synthesis of Metal NPs

Metallic nanoparticles (MNPs), either in their pure form or combined with another metal (bimetallic) have gained exclusive interest, due to their broad usage in various fields of science and technology (Förster *et al.,* 2012). The synthesis of MNPs is usually achieved by employing physical (e.g., laser ablation, condensation, lithography), chemical (chemical reductants), or biological (e.g., microorganisms, plants) techniques (Kiranmai, 2017; Vaid *et al.,* 2020) (figure 2.1). Some of these procedures are easy to execute and permit control of the crystallite size by altering the environment of the reaction. The selection of a synthesis method for MNPs is significant because, during formulation, procedures like the kinetics of interaction of the metal ions with reducing agent, the adsorption process of stabilizing agent with metal NPs, and various experimental techniques produce a strong influence on the NPs physicochemical properties such as morphology, size, charge, and dispersity (Jamkhande *et al.*, 2019). Additionally, it is crucial to employ a procedure that is easy to execute and cost-effective;uses non-toxic/benign compounds; and can be applied in large-scale production (Dhall and Self, 2018).

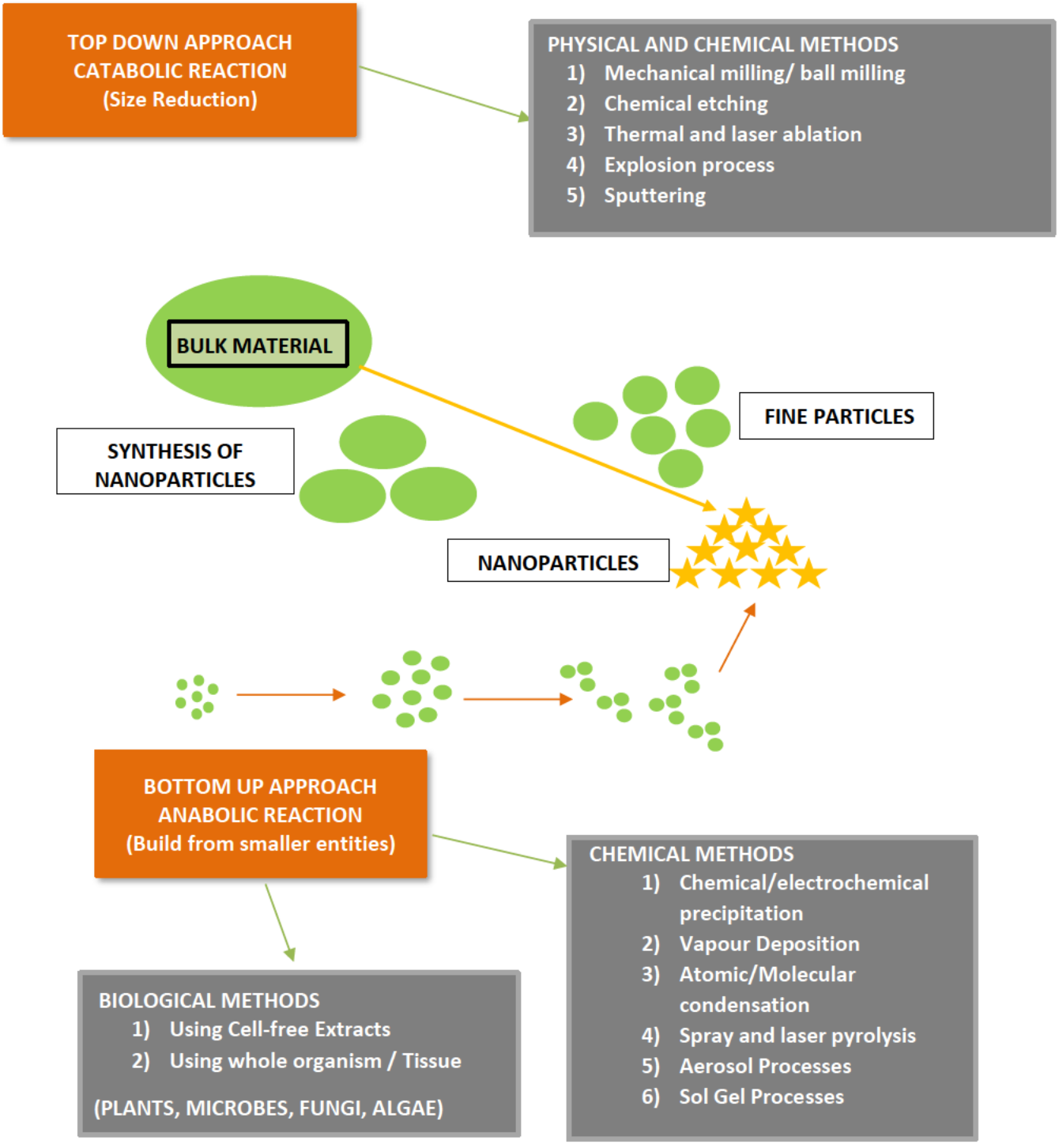

Figure 2.1: An illustration of the diverse methods used to synthesize nanoparticles (Vaid *et al.*, 2020)

2.3.1 Physical Methods

Physical methods that are commonly used for the synthesis of MNPs are laser ablation, evaporation-condensation, and lithography. The laser ablation synthesis method is a practical and efficient procedure to prepare and obtain metal colloids without the excessive use of chemical substances (Fazio *et al.*, 2020). The method permits a change in the number of pulses for a controlled formation of the colloid's particle size. It uses a standard high-power laser and a small laser beam spot sizer, which produce small NPs with a narrow size distribution in pure water without the presence of chemicals, thus making it an environmentally friendly method (Güzel and Erdal, 2018). The drawback, on the other hand, is that the concentration of the resulting NP colloids is frequently too low, making it problematic to utilize them on an industrial scale. To counteract the low concentration yield of the colloids for final applications, high-energy lasers need to be employed. Though high-energy lasers are used as alternatives, their application is usually limited by high costs, as these lasers are more expensive than standard lasers (Sportelli *et al.*, 2018).

Evaporation-condensation is another physical method that can be used to fabricate MNPs. The technique is usually performed through a transferred direct current arc, which delivers the energy required for the metal target evaporation. In order to avert oxidation of the particles during the procedure, the formulation process is performed in an atmosphere of inert gases (Förster *et al.*, 2012). This method permits the direct synthesis of NPs utilizing pure metals as the initial materials, thus averting reactions that are expensive and with potentially poisonous outputs (Förster *et al.*, 2012; Vodop'yanov *et al.*, 2017). Using this method is limited by the large amount of space occupied by thetube furnace, leading to high energy consumption by increasing the environmental temperature around the source material. Furthermore, it is time-consuming as it takes a long time before thermal stability is achieved (Vodop'yanov *et al.*, 2017).

Moreover, MNPs can also be physically synthesized using the nanosphere lithography (NLS) technique**.** Through the years, NSL has enticed increasing attention owing to its compatibility with wafer-scale procedures; its ability to produce a broad range of

homogeneous nanostructures, and its cost-effectiveness (Colson *et al.*, 2013*;* Zaleska-Medynska, 2018; Brady *et al.*, 2019). The technique combines the advantages of both top-down and bottom-up approaches. During the top-down technique, bulk material is physically broken down to make smaller molecules, whereas the bottom-up approach relies on nucleating atomic-sized materials into the eventual nanoparticles (Colson *et al.,* 2013). Moreover, the bottom-up approach is carried out in a two-step process that includes the preparation of a colloidal crystal mask (CCM) made of nanospheres and the deposition ofthe desired material through the CCM mask (Colson *et al.,* 2013). The mask is then removed, and the layer keeps the ordered patterning of the mask apertures. However, this technique is limited by the lack of structural variety, since it only produces triangular-shaped NPs (Colson *et al.*, 2013). In addition, the difficulty of the method together with the extreme costs of the equipment deems the lithographic techniques unfavorable for numerous researchers.

2.3.2 Chemical Method

The chemical reduction method is one of the most used synthesis approaches for MNPs. This approach utilizes either inorganic or organic reducing substances such as ascorbic acid, sodium citrate, sodium borohydride, polyol process, elemental hydrogen, ammonium formate, and hydrazine to reduce metal ions to their nanoparticles (Iravani *et al.,* 2014; Güzel and Erdal, 2018). The MNPs produced by this technique possess well-defined dimensions, sizes, structures, and composition, and thus can be employed in various research areas such as drug delivery: imaging and sensing; diagnosis. However, the use of this method is sometimes limited by its use of toxic chemicals; its expensive cost, and high strenuousness (Modan and Plăiașu, 2020). Thus, there is a need for the identification and use of environmentally safe, low-cost, easy-to-use methods.

2.3.3 Biosynthesis Method

The biosynthesis of NPs is currently the method receiving abundant attention because of the increasing necessity to produce NPs that are environmentally safe and cost-effective (Rahimi and Doostmohammadi, 2019). In the last couple of years, various researchers have investigated and reported on the extracellular production of stable MNPs using

bacteria, fungi, actinomycetes, as well plant extracts (Mikhailov and Mikhailova, 2019; Pyrzynska and Sentkowska, 2021; Saravanan *et al.*, 2021). Plant extracts have been extensively used for the synthesis of MNPs owing to their possible medicinal benefits, abundant availability, and faster rate of NP production (Hosseini Bafghi *et al.*, 2021; Krishnaraj *et al.*, 2022). The parts of the plants that are extracted and used during the synthesis of the MNPs are usually the fruits, flowers, leaves, roots, and seeds (El-Seedi *et al.*, 2019; Ishak *et al.*, 2019; Jadoun *et al.*, 2021; Naikoo *et al.*, 2021). A study by Sorbiun *et al.* (2018), reported that biomolecules such as phenols, proteins, enzymes, vitamins, alcohols, amino acids, terpenoids, polysaccharides, proteins, flavones, and alkaloids which are found in plants, are the ones predominantly accountable for the reduction of metal ions into stable MNPs (Sorbiun *et al.*, 2018; Vaid *et al.,* 2020). For this study, bimetallic colloidal SeAgNPs were synthesized using an aqueous extract from fenugreek seeds.

Fenugreek (*Trigonella foenum-graecum* L.) is one of the oldest medicinal plants from the Fabaceae family originating in central Asia 4000 years Before Christ (B.C). Its description and benefits had been reported in the Ebers Papyrus (one of the oldest maintained medicinal documents) earlier in 1500 BC in Egypt (Ahmad *et al.*, 2016; Anitha *et al.,* 2021). Fenugreek seeds contain a variety of biomolecules or compounds including antioxidants such as flavonoids, alkaloids, and saponins; and phenolic constituents like gallic acid, protocatechuic acid, catechin, gentisic acid, chlorogenic acid, vanillic acid and syringic acid which possess biological activities such as anticancer, antiviral, antidiabetic, anti-inflammatory, antimicrobial, and anticholesterolemic properties (Kor and Moradi, 2013; Almatroodi *et al.,* 2021).

2.4 Stabilization and Functionalization

The successful biological use of metal NPs as chemotherapeutic agent-delivery vectors significantly depends on them having exceptional stability, reduced toxicity, and site specificity (Abdellatif *et al.,* 2021). To achieve this, following synthesis, NPs usually need to be functionalized with non-toxic biomolecules such as polymers/ and targeting agents

(Luesakul *et al.*, 2018; Maiyo and Singh, 2019). The coating of NPs with polymers ensures the preservation of the NPs unique properties and increases the NP's viscosity to enhance colloidal stability which leads to less interaction between the NPs (Lee *et al.,* 2021). This results in hindering any further growth or structural changes; and prevents agglomeration or precipitation upon administration which enhances their uptake by the tumor cells (Sharma *et al.*, 2019; Duan *et al.*, 2020). Various polymers have been previously used to stabilize metal NPs including cellulose, starch, polyethylene glycol (PEG), poly (ethyleneimine) (PEI), poly(L-lysine) (PLL), poly(d,l-lactide-co-glycolide) (PLG), dendrimers, dextran, and chitosan; and amongst these, chitosan and PEG have been extensively used (Xu *et al.,* 2015; Hefni *et al.,* 2016; Wang *et al.,* 2018).

Chitosan (Ch) is a natural positively charged polymer with great biological properties such as high bio adhesiveness, biodegradability, biocompatibility, antibacterial activity, low cytotoxicity, and immunogenicity (Collado-González *et al.,* 2017). Due to the cationic nature of this polymer, it can adsorb onto the surface of the metal NPs stabilizing and tailoring them for the binding of therapeutic agents. Ch binds and protectstherapeutic drugs from degradation by intracellular enzymes. Ch-tailored NPs can interact with negatively charged membranes of various cells and facilitate effective cellular uptake. Ch also facilitates the intracellular circulation time of the NPs and further controlsthe steady cytosolic release of the therapeutic drugs due to its high buffering capacity (Richard *et al.,* 2013; Collado-González *et al.,* 2017; Parhi, 2020; Aibani *et al.,* 2021). Polyethylene glycol (PEG) is an inert, non-toxic, biocompatible, amphiphilic, easily excreted polymer that is usually used as a co-polymer to coat the surface of NPs. The PEG coat functions as an armor shielding the encapsulated therapeutic drugs from enzyme degradation, instant renal clearance, and interacts with cell surface proteins, thus decreasing distasteful immunological effects (Xiao *et al.,* 2011; Wang *et al.,* 2018; Liu *et al.,* 2019). These features are essential for the successful application of NPs and drug- loaded nanocomplexes *in vivo.*

Furthermore, the polymers provide a surface that can host numerous biomolecules (anticancer drugs or genes) at a time and can be synthetically modified with targeting

ligands that are essential for targeted drug-delivery (Cordani and Somoza, 2019). The targeting ligands are covalent/non-covalently conjugated onto the surface of MNPs and are complementary to the receptors expressed on the targeted cells, allowing for effective delivery of the attached biomolecules to the specific cells with minimal damage to the surrounding areas (Bazak *et al.,* 2015). Receptors that are commonly expressed on cancer cells include transferrin receptors, folate receptors, glycoprotein (such as lectin), and epidermal growth factor receptors to name a few (Zeromski, 2002). Amongst these, folate receptors are the most overly expressed in many tumors particularly breast (MCF-7), and cervical (HeLa) cells (Weitman *et al.,* 1992). The folate receptors (FA-Rs) (glycophosphatidylinositols membrane proteins) affiliate with the ligand FA, which is small, non-immunogenic, readily available, biodegradable, and easily conjugated to other biomolecules. In addition, FA can regulate replication, cell growth, and protein synthesis.

FA enables the NPs' drug delivery through active targeting which is better known as targeted drug delivery (Bazak *et al.,* 2015). The process provides several advantages over non-targeted drug-delivery vectors including increasing transfection to specific sites and increasing the quantity of the drug delivered to the targeted cells, therefore, lessening or avoiding possible systemic toxicity, which causes undesirable side effects (Yang *et al.*, 2018). Upon the entry of FA-conjugated NPs into the targeted cells via receptor-mediated endocytosis, the NPs cause S phase arrest, a form of cell cycle arrest and further orchestrates mitochondrial-mediated apoptosis (Pi *et al.*, 2013). This is achieved by inducing reactive oxygen species (ROS) production which disrupts the mitochondria until cell death, further disorganizing the cytoskeleton through F-actin expression reduction. This approach has significantly expanded the therapeutic windows of drugs by allowing for efficient and safe targeting of specific cells/tissues.

2.5 The Mechanism of Action of Cancer Targeting MNPs

MNPs have been reported to get to the outer membrane of a cell and intermingle with components of the plasma membrane or extracellular matrix then go into the cell, generally through endocytosis due to their unique tunable physicochemical properties

(Cordani and Somoza, 2019; Rennick *et al.,* 2021). Depending on the cancer cell type, as well as the proteins, lipids, and other molecules involved in the process, endocytosis can be classified into several types. These include phagocytosis, clathrin-mediated endocytosis, and caveolin-mediated endocytosis. Furthermore, the structural composition of the NPs also plays a role in deciding which mechanism of entry occurs (Vaid *et al.,* 2020). For instance, small targeted specific NPs enter the cell through caveolin-receptor-mediated uptake pathways, while the large/bulk/aggregated NPs enter through clathrin receptor-mediated, phagocytosis or endocytosis uptake mechanisms (Rennick *et al.,* 2021).

Following successful targeting, binding, and the internalization of the NPs by one of the mentioned pathways the MNPs either interact with intercellular proteins or get sequestrated within the endosome vacuole, followed by maturation to lysosomes (Cordani and Somoza, 2019). This is then followed by their degradation, alteration, or dissociation before being released into the cytosol. This is enabled by the cancer cells' acidic pH microenvironment with redox imbalance that subsequently leads to pro-oxidant conversion of the MNPs activating the supplementary formation of free radicals/ROS (Khurana *et al.*, 2019). This affects the physiology of the cell resulting in the disruption of the mitochondrial (Mt) membrane initiating leakage of Mt proteins and endoplasmic reticulum (ER) stress-activating pathways that lead to the programmed death of cancer cells either by autophagy, apoptosis, or necrosis (figure 2.2) (Khurana *et al.*, 2019; Ikram *et al.,* 2021; Miranda *et al.*, 2022).

The multiple molecular pathways activated by the ROS-induced intracellular stress to induce autophagy include but are not limited to the nuclear factor kappa B (NFκB), phosphatidylinositol-3-kinase (PI3K/Akt), mammalian target of rapamycin (mTOR), canonical Wnt (Wnt/β-catenin), and mitogen-activated protein kinase/extracellular-signal-regulated kinase (MAPK/Erk) pathways. The NFκB pathway stimulates inflammatory and oxidative stress signaling, which disrupts cellular homeostasis (Panzarini *et al.,* 2015; Khurana *et al.*, 2019). Whereas, the PI3K/Akt/mTOR, MAPK/Erk, VEGF, and Wnt/β-catenin pathways are essential in oncogenic signaling and their

modulation by the MNPs causes compromised cellular proliferation which hinders growth and encourages signaling in the locality of the tumor microenvironment.

The pathways leading to apoptosis include intrinsic and extrinsic apoptosis triggered by the generated ROS upon the conformational alterations of the mitochondrial membrane (Mohammadinejad *et al.,* 2019; Vaid *et al.,* 2020). The intrinsic pathway is activated by the release of cytochrome-c (Cyt-c) in the cytosol, which binds with pro-caspase-8 and apoptotic protease factor -1 (Apaf-1), activating the caspase-9/3 apoptotic mechanism and initiating apoptosis by cleaving the cytoplasmic and nuclear substrates (Poly ADP-ribose Polymerase-1 or PARP-1). Extrinsic apoptosis is activated by the signaled activation of pro-caspase-8 which starts apoptosis by cleaving other caspases. Furthermore, for necrosis to occur the NPs signal the activation of receptor-interacting serine/threonine-protein kinase 3 (RIPK3) and receptor-interacting serine/threonine-protein kinase 1 (RIP1/RIP1). These pathways then affect the mitochondria by increasing the production of nicotinamide adenine dinucleotide phosphate (NADPH) oxidase and cellular calcium (Ca2+) thus triggering ROS production and influx leading to induced programmed necrosis (Bauer *et al.,* 2011; Manke *et al.,* 2013; Vaid *et al.,* 2020).

The resultant cellular morphological changes caused by autophagy, apoptosis, and necrosis include loss of membrane integrity, nuclear fragmentation, chromatin condensation, cytoplasmic shrinkage, and structural configuration of cytoplasmic organelles, which can be observed microscopically (Nikoletopoulou *et al.,* 2013). The occurrence of these disruptive cellular events is dependent on the type of cell, as well as the size and dose of the metal NPs used (Vergallo *et al.,* 2016; Khurana *et al.*, 2019).

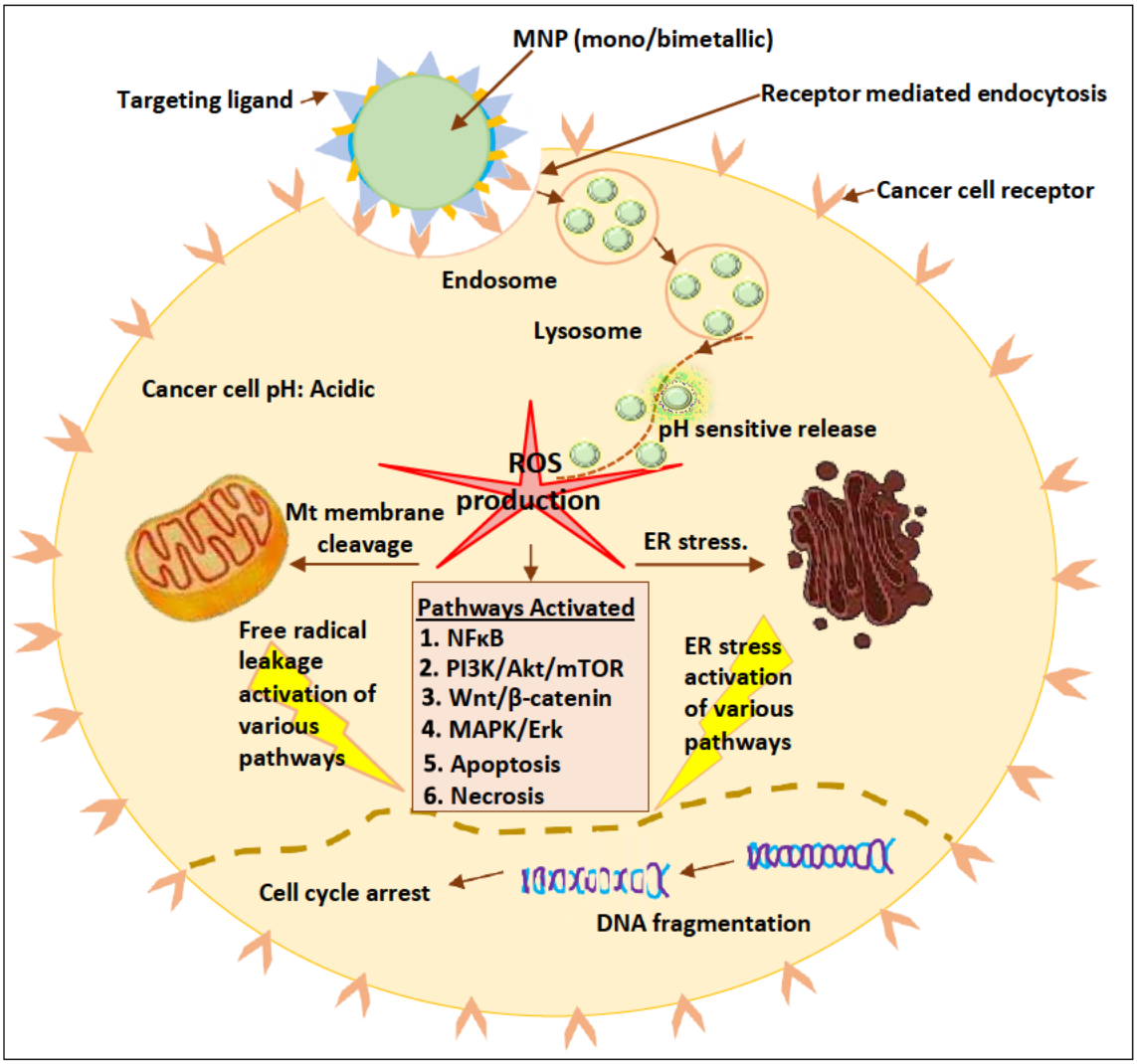

Figure 2.2: An illustration of the receptor-mediated cellular uptake of targeted MNPs and the anticancer mechanism of action (adapted from Ikram *et al.,* 2021)

2.6 Application of MNPS (Se, Ag and Bimetallic NPs) in Cervical Cancer Therapy

The delivery of anticancer agents/drugs using MNPs in cervical cancer therapy has been conducted *in vitro* and *in vivo* with different outcomes indicating their potential efficiency. Over the years, many studies have been reported. For instance, Srivastava and Kowshik (2016) reported on Se NPs that were biologically formulated using the halophilic bacterium, *Idiomarina* sp. PR58-8 and sodium selenite as the precursor. The results depicted that the Se NPs displayed selectivity in causing cytotoxicity towards the human cervical cancer cell line, HeLa, while being non-toxic towards the model normal cell line, HaCaT. The Se NPs induced caspase-dependent apoptosis in HeLa cell lines. These results

suggested the application of Se NPs synthesized by *Idiomarina* sp. PR58-8 as potential anti-neoplastic agents (Srivastava and Kowshik, 2016).

In another study, Yuan *et al.* (2018) reported on the delivery of camptothecin (CPT) using biosynthesized (sinigrin) Ag NPs in human cervical cancer cells. The researchers found that the Ag@CPT NCs treatment notably inhibited cell viability and proliferation of the HeLa cells, increasing the levels of oxidative stress markers and decreasing antioxidative stress markers compared to free CPT treatment. Furthermore, the merged treatment upregulated numerous proapoptotic gene expressions and downregulate antiapoptotic gene expressions. Intriguingly, the merged treatment modulated a variety of cellular signaling molecules involved in cell survival, cytotoxicity, and apoptosis. These findings suggested that the Ag@CPT NCs caused cell death by inducing the mitochondrial membrane permeability change and activation of caspase 9, 6, and 3. The synergistic cytotoxicity and apoptosis effect seemed to correlate with increased ROS formation and depleted antioxidants. Overall, the results suggested that the combination of CPTand Ag NPs could provide a beneficial effect in the treatment of cervical cancer compared to the monotherapy (Yuan *et al.*, 2018).

Xia and colleagues (2018) carried out a study on the anticancer drug-delivery activity of folic acid-targeted DOX-loaded chemically synthesized Se NCs (FA-Se@DOX NCs). The NCs were tested on folate receptor-positive human cervical carcinoma (HeLa) cells and folate receptor-negative lung cancer (A549) cells. The FA-Se@DOX NCs displayed substantial cellular uptake in HeLa cells in comparison with A549 cells; and entered the HeLa cells mostly by the folate receptor-mediated endocytosis pathway. In comparison to free DOX or Se@DOX NCs at the equivalent dose of DOX, FA-Se@DOX NCs demonstrated apparent activity to prevent HeLa cells' proliferation and induce apoptosis in HeLa cells. More significantly, it was observed that the FA-Se@DOX NCs could specifically accumulate in the tumor site, which contributed to the significant antitumor efficacy of FA-Se@DOX NCs *in vivo*. The study suggests that the FA-Se@DOX NCs may be a novel therapeutic candidate for human cervical carcinoma therapy (Xia *et al.*, 2018).

In another study, Xia and colleagues (2020) reported on the capability of chemically synthesized RGDfC peptide-tagged Se NPs to deliver siRNA gene in selected cancer cell lines. The findings demonstrated that the RGDfC-Se@siRNA exhibited greater uptake in HeLa cervical cancer cells in comparison to human umbilical vein endothelial cells (HUVECs). The RGDfC-Se@siRNA entered the HeLa cells via receptor-facilitated endocytosis and demonstrated faster siRNA release in a cancer cell microenvironment in comparison with a normal physiological environment. As a result, the system inhibited the invasion, migration, and proliferation of the HeLa cells, and triggered cell apoptosis. Furthermore, RGDfC-Se@siRNA stimulated the distraction of mitochondrial membrane potentials. The system improved the generation of ROS in the HeLa cells, indicating that the mitochondrial dysfunction mediated by ROS might play a significant role in RGDfC-Se@siRNA-induced apoptosis. The results indicated that RGDfC-Se@siRNA provided a promising potential for cervical cancer therapy (Xia *et al.,* 2020).

In a recent study by Iqbal *et al.* (2022), Ag NPs were biosynthesized using a variety of peach plant (PP) leaf extracts (Wild type, Carmon, Indian Blood). The NPs were tested on a normal pre-osteoblast cell line (MC3T3) and two cancer cell lines (HeLa and HepG2). The NPs had a positive effect on the MC3T3 cells as they enhanced the growth of the cells while demonstrating a concentration/dose-dependent inhibitory effect on the growth of the two cancer cells. All the formulated Ag NPs showed a distinct cytotoxic effect against HeLa and HepG2cell lines. The findings suggested that the Ag NPs produced from PP extracts are effective against the cancer cells, while simultaneously being non-toxic to normal non-cancer cells (Iqbal *et al*., 2022).

Currently, a limited number of studies on the application of bimetallic NPs (BMNPs) in cervical cancer treatment have been reported. For instance, Alshatwi and co-workers (2015) investigatedthe anticancer activity of green synthesized bimetallic Au@ Pt NPs against human cervical cancer cells (SiHa). The findings showed that the Au@Pt NPs induced cell death/apoptosisthrough the G2/M phase checkpoints in dose- and time-dependent means (Alshatwi *et al.,* 2015).

In 2021, Ghosh and Singh reported on the anticancer activity of the biogenically synthesized *Desmodium gangeticum* Au-Ag NPs against HeLa cells. The findings showed that the antiproliferative effect of the synthesized BMNPs was dose-dependent and was through the passive targeting of the HeLa cells, causing destruction to the mitochondria membrane, which resulted in the induction of apoptotic cell death through the ROS-mediated caspase pathway activation. These findings suggested the application of *Desmodium gangeticum* synthesized Au-Ag NPs as potential anti-cancer agents (Ghosh and Singh, 2021). That said, more studies need to be done to fully explore the application and mechanisms of action of BMNPs in cancer treatment.

III. Chapter Three: Materials and Methods

3.1 Materials

The human cervical cancer (HeLa) cells and embryonic kidney cells (HEK293) were purchased from Merck (St Louis, MO, USA). The maintenance and sub-culturing of the cells were carried out as previously described (Singh and Ariatti, 2003). Fenugreek seeds were purchased at Dischem (South Africa). The anticancer drug doxorubicin hydrochloride (DOX. HCl, Mw 579.98 g mol-1), N'-hydroxysuccinimide (NHS), N'-dicyclohexyl-carbodiimide (DCCI), trypsin-versene, ascorbic acid ($C_6H_8O_6$), Minimum Essential Medium (EMEM) with Earle's salts and L-glutamine, penicillin (500 units/ml)/streptomycin (5000 µg/ml), sodium borohydride ($NaBH_4$), phosphate buffer saline (PBS), dimethyl sulphoxide(DMSO), benzolylated dialysis tubing (MWCO 12000 Da), sodium selenite (Na_2SeO_3), selenious acid (H_2SeO_3), polyethylene glycol1000 (PEG, Mw 1000), chitosan, silver nitrate($AgNO_3$), MTT, folic acid ($C_{19}H_{19}N_7O_6$), polyvinylpyrrolidone (PVP, Mw 40,000), 1-(3- dimethylaminopropyl)-3-ethylcarbodiimide (EDC), fetal bovine serum (FBS), acridine orange/ethidium bromide (AO/EtBr) dye (100 µg ml^{-1} acridine orange and 100 µg ml^{-1} ethidium bromide), were purchased from Merck (South Africa). All other chemicals were of analytical grade and were purchased from Merck (South Africa).

3.2 Methods

Synthesis of Bimetallic Selenium-Silver Chitosan PEGylated Folic Acid Nanoparticles (SeAgChPEGFA NPs):

3.2.1 Chemical Synthesis of SeAg NPs

The colloidal bimetallic SeAg NPs were synthesized by the co-reduction of sodium selenite (Na_2SeO_3) and silver nitrate ($AgNO_3$) solutions, with the aid of sodium borohydride ($NaBH_4$) as the reducing agent and polyvinylpyrrolidone (PVP) as a stabilizer as described previously (Wang *et al.*, 2009; Zhang and Toshima, 2013) with slight modifications (figure 3.1 a). Where, a 60 ml PVP aqueous solution (1 mM) was mixed with an aqueous solution of Na_2SeO_3 (20 ml, 5 mM) and stirred for half an hour under nitrogen (inert) conditions. Subsequently, an aqueous solution of $AgNO_3$ (20 ml, 1 mM) was introduced into the reaction mixture, followed by the addition of an aqueous solution of $NaBH_4$ (5 ml, 10 mM), and apH adjustment of the resultant solution mixture to pH 4.7. The mixture was then vigorously stirred overnight under nitrogen conditions, which resulted in a change in colour from a colourless solution to glossy orange suggesting the synthesis of bimetallic SeAg NPs.

3.2.2 Biosynthesis of SeAg NPs

3.2.2.1 Seed Extract Preparation

The fenugreek seeds were washed with sterile de-ionized water to eliminate dust particles and 10 g of fine-grinded seeds were placed in a beaker with 500 ml of distilled water as previously described (Alagesan and Venugopal, 2019). The mixture was heated for 15 minutes (min) till the colourless solution changed to goldish-yellow. The mixture was then cooled at 25˚C and filtered with filter paper (Whatman no. 1) before being centrifuged at 1500 revolutions per minute (rpm) for 5 min to eliminate the biomaterials. The resultant fenugreek seed extract (F-) was then stored at 25 °C to be used for further experiments (Alagesan and Venugopal, 2019).

3.2.2.2 NPs Synthesis

The NPs were synthesized as previously described (Elemike *et al.,* 2019) with slight modifications (figure 3.1 a). Initially, 50 ml of seed extract was mixed with 25 ml of 30 mM selenious acid and 25 ml of 1 Mm silver nitrate and was left to stir. The solution was stored at 25°C for 1 hour. The reaction mixture was then evaluated for any changes in colour and examined periodically by a UV-Vis spectrophotometer. Thereafter, the formulated F-SeAg NPs were collected by centrifuging the mixture at 1500 rpm. The resultant nano pellets were then washed with distilled water and acetone, and they were dried overnight. For use in further analysis, the F-SeAg NPs were resuspended in PBS (pH 7.4) by ultrasonication and centrifuged.

3.2.3 Synthesis of SeAgChPEGFA@DOX-Loaded Nanocomplexes

The SeAgChPEGFA NPs from both methods of synthesis were prepared as previously described (Maiyo and Singh, 2019) with slight modifications (figure 3.1 a). Briefly, to make SeAgChPEGNPs, 100 ml of 0.2% Ch (in 1% acetic acid, CH_3COOH) + 0.8% PEG solution (in 1% acetic acid) was prepared and left to stir for 12 hours. Thereafter, 10 ml of the solution mixture was placed into 2 separate flasks and used to coat the SeAg NPs from both methods of synthesis and were left to stir for 48 hours. Upon completion, the produced NPs underwent dialysis (MWCO 12 kDa) against deionized water for 24 hours and stored at 4°C for impending use. Moreover, to make SeAgChPEGFA NPs, a FA (20 mg), 20 ml DMSO and DCCI (100 mg) solution, was prepared initially and then stirred for 2 hours at 37 ˚C. Then, 100 ml of Ch + PEG solution (in 1% acetic acid) solution was slowly introduced to the FA solution, pH adjusted (9.0) and the mixture was stirred for a further 24 hours. Then, 20 ml of the solution mixture was placed in 2 separate flasks and used to coat SeAgNPs (left to stir for 48 hours). Upon completion, the produced NPs underwent dialysis (MWCO 12 kDa) against deionized water for 24 hours and at 4°C for future use.

The conjugation of DOX onto the polymer-capped NPs surface was through an adsorption and amide binding of the succinyl-activated DOX's negative hydroxyl groups to the positive amine groups of chitosan. Therefore, DOX-loaded nanocomplexes (NCs) were formulated as described previously (Xia *et al.*, 2020) with slight modifications (figure 3.1

b). Where, 2 mg DOX·HCl was liquified in EDC + NHS (1 %) to activate the drug, thereafter the activated DOX solution was added dropwise into the prepared selenium NP solution ~1:1 $^{v}/_{v}$ and then stirred for 8 hours at 37 °C. The resultant DOX-loaded NCs were dialyzed for purification (MWCO 12 kDa) in deionized water for 6 hours.

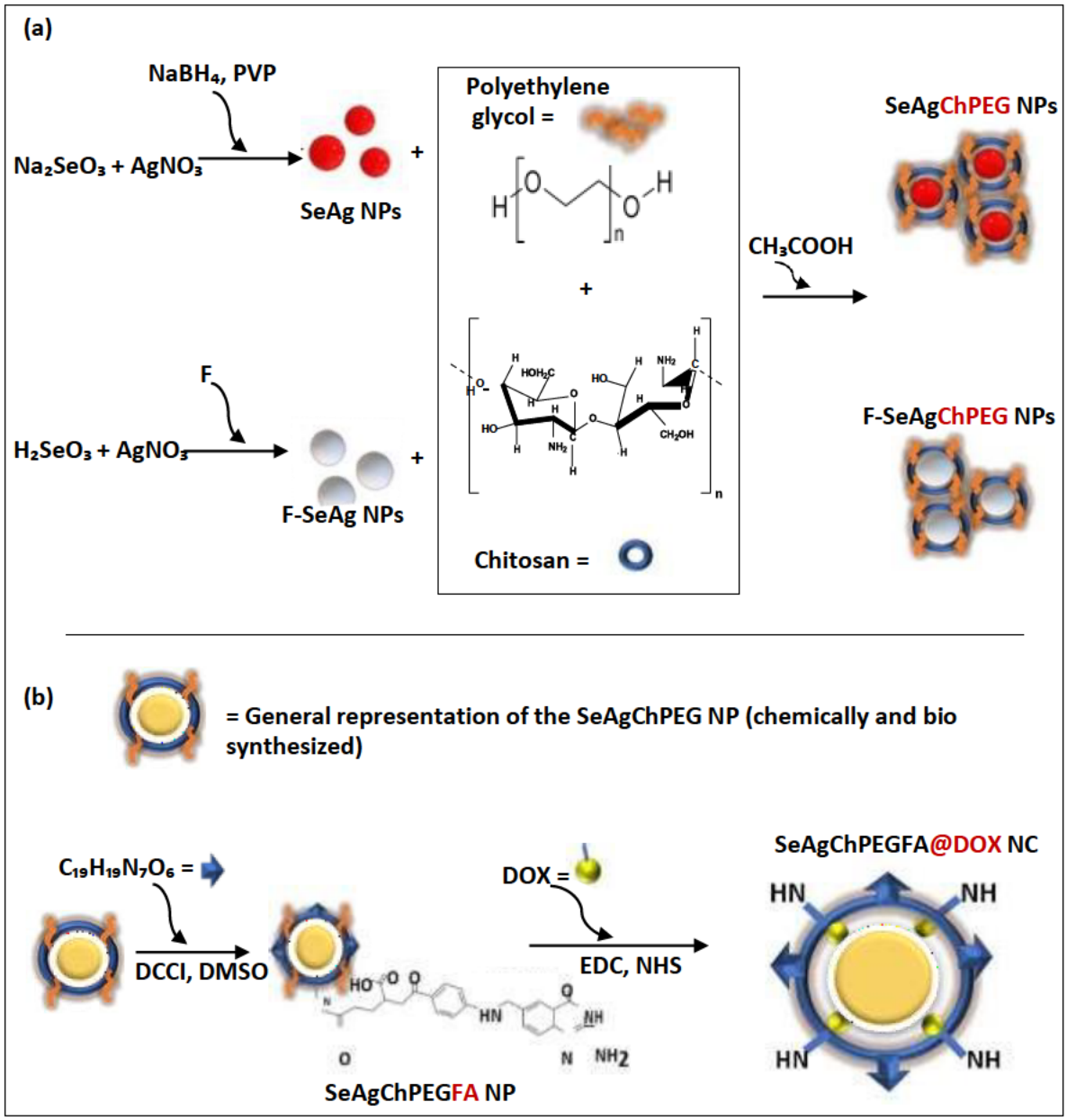

Figure 3.1: The chemical synthesis and biosynthesis mechanisms and conjugation of Ch-PEG co- polymers on the SeAgNPs and F-SeAgNPs (a); and the general folic acid and DOX bioconjugation on the SeAgChPEG NPs (b) (Adapted from Malinga *et al.,* 2021).

3.2.4 Characterization

3.2.4.1 UV-vis Spectroscopy, TEM, *Zeta* Potential, and FTIR Spectroscopy

The successful formulation and surface functionalization of the NPs was substantiated by employing the UV-visible (Cary 60 UV-Vis, Agilent, Santa Clara, USA), and FTIR (ATR, PerkinElmer Inc., Waltham, USA) spectrometer. Morphology plus the scattering of the NPs were assessed by making use of a transmission electron microscope (JEOL JEM-1010, JEOL, Tokyo, Japan). The size and stability were evaluated using a *zeta* potential analyzer (Litesizer 500, Anton Paar, Graz, Austria).

3.2.4.2 Drug Binding Percentage Evaluations

The drug loading percentage (DL%) and the encapsulation efficiency percentage (EE%) of DOX of the chemically synthesized SeAgChPEGFA NPs and biosynthesized SeAgChPEGFA NPs were assessed by centrifugation of the colloidal system at 21000 rpm at 25 ˚C for 30 minutes. Free DOX aliquots in the resultant supernatants obtained following centrifugation were determined by UV-vis spectroscopy at a wavelength of 481 nm. The DL% and EE% were calculated as follows (Small Jr *et al.*, 2017; Tempfer *et al.*, 2018):

$$DL\ (\%) = \frac{Weight\ of\ drug\ in\ nanoparticles}{Weight\ of\ nanoparticles}\ X\ 100$$

$$EE\ (\%) = \frac{Weight\ of\ drug\ in\ nanoparticles}{Weight\ of\ total\ drug\ used}\ X\ 100$$

3.2.4.3 *In Vitro* Release

The ability of the formulated NPs to release the drug cargo *in vitro* was assessed as described previously (Xia *et al.*, 2018). Summarily, 2 ml of SeAgChPEGFA@DOX and F-SeAgChPEGFA@DOX NCs were placed into separate dialysis tubes/cylinders (MWCO 12 kDa). Then the cylinders were transferred into 10 ml phosphate buffer saline (PBS) with various pHs (4.4, 5.4, or 7.4), and incubated at 25°C for 48 hours. This was followed by the seeding of 5 µl of each sample out from the PBS at various times from 0 – 72 hours and analyzed. The concentrations of DOX released were quantitatively established by UV-vis spectroscopy at 535 nm.

3.2.5 Cell Culture and Maintenance

Cancer and non-cancer cells were preserved and proliferated at 37 °C and 5% CO^2, in 25 cm^2 flasks comprising of sterile EMEM, FBS (10%, *v*/*v*, penicillin G (100 U/ml), and streptomycin sulphate (100 µg/ml). The cells were divided into precise ratios for required analysis purposes and the medium changed routinely.

3.2.6 Cytotoxicity Studies

Initially, the non-cancer (HEK293) and cancer (HeLa) cells were sub-cultured and preserved as described earlier (Singh and Ariatti, 2003). Thereafter, the cytotoxicity profiles of the NPs/NCs were evaluated in these cells using an MTT assay (Akinyelu and Singh, 2019). The selected cell lines were aliquoted in 96-well plates at densities of 1.76 x 10^6 and 1.64 x 10^6 cells/well, respectively, and incubated at 37 °C for 24 hours. After the cell's incubation, the old medium was replaced with fresh medium followed by the addition of 0.3 ml of the NPs/NCs prepared at different concentrations (5, 10, 15, 20, and 25 µg/ml), and the cells were incubated at 37 °C for a further 48 hours. Afterward, the older medium was replaced with renewed medium + 10% MTT agent (prepared in 5 mg/ml PBS), and then stored at 37 °C for 4 hours. The fresh medium + 10% MTT agent mixture was subsequently removed, and the cells were washed with PBS (2 × 0.3 ml) and treated with 0.3 ml of DMSO. Lastly, the absorbance values were measured at 570 nm. The cytotoxicity was compared to the untreated cells (control) (100%). The average absorbance measurements were changed into a percentage (%) of cell viability, as per the equation below (Carlson *et al.*, 2012):

$$Cell\ viability\ (\%) = \frac{Absorbance\ of\ treated\ cells}{Absorbance\ of\ untreated\ cells}\ X\ 100$$

3.2.7 Anticancer Studies

The apoptosis activity profiles of NPs/NCs were studied as previously described (Maiyo and Singh, 2019). Succinctly, the HEK293 and HeLa cells were aliquoted at densities of 1.26 x 10^6 and 1.7 x 10^6 cells/well, correspondingly into 12-well plates, and incubated for

24 hours at 37 °C. Subsequently, the cells were then treated with the NPs/NCs and incubated at 37 °C for another 24 hours. The cells were then washed with PBS (100 µl) and stained with AO/ETBR dye (10 µl). A fluorescent microscope (OLYMPUS) at X200 magnification was used to study the apoptosis activities of the NPs/NCs and the apoptotic Index was calculated using the formula below:

$$Apoptotic\ Index\ (AI) = \frac{Number\ of\ Apoptotic\ Cells}{Total\ Number\ of\ Cells}$$

3.2.8 Statistical Analysis

The studies on biologically evaluating the NPs and NCs were performed in triplicates, and the results were disclosed as mean ± standard deviation (SD). A one-way ANOVA and Tukey's multiple comparison tests were used to evaluate the statistical significance. Statistically substantial values are represented by $*p < 0.05$, $**p < 0.01$, $***p < 0.001$.

IV. Chapter Four: Results and Discussion

4.1 Synthesis and Characterization

4.1.1 Synthesis

MNPs are exceptionally known for their unique properties, especially the optical characteristic they possess, which is because of the localized surface plasmon resonance (LSPR) (Grzelczak *et al.,* 2008). Therefore, the successful synthesis of the BMNPs was validated with the change in colour, UV-vis, and FTIR spectroscopy.

The BMNPs were successfully synthesized (chemically and biosynthetically) by the co-reduction process. This was exhibited by the reaction mixture's change in colour from cloudy to a glossy reddish-orange and from yellow-gold to orange-brown, indicating the formation of SeAg NPs and F-SeAg NPs, respectively, as shown in figure 4.1 (images e and c). The change in colour can be attributed to the reduction of Se-Ag metal ions from sodium selenite and silver nitrate into BMNPs by sodium borohydride (in the case of chemical synthesis) (Mavani and Shah, 2013; Sithole *et al.,* 2018) and active biomolecules found in the fenugreek seed aqueous extract (in the case of biosynthesis) (Mavani and Shah, 2013; Sithole *et al.,* 2018). According to a previous study, the colour of metal NPs is attributable to the excitation of LSPR arising from the collective oscillation of free conduction electrons induced by an interacting electromagnetic field (Grzelczak *et al.*, 2008). These findings correspond with similar studies on each of the metal NPs (Jana *et al.,* 2016; Krishnaraj *et al.*, 2022).

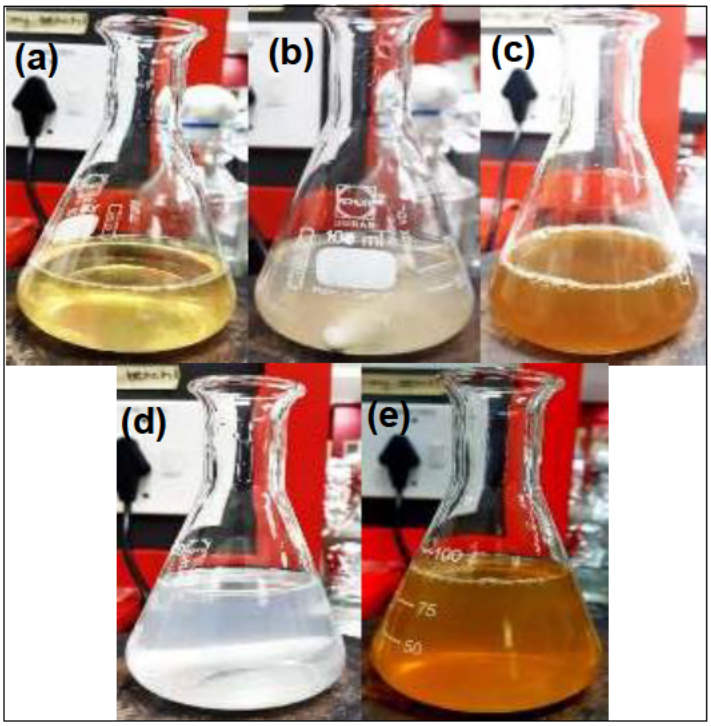

Figure 4.1 (a – e): Synthesis images of bimetallic NPs where; (a) Fenugreek seed extract (F), (b) Selenious acid + silver nitrate, (c) F- SeAg NPs, (d) Sodium selenite + silver nitrate + PVP + $NaBH_4$ and (e) SeAg NPs.

4.1.2 UV-vis Spectroscopy

To verify the synthesis, stabilization with selected polymers, and functionalization, with selected biomolecules (e.g., folic acid, and anticancer drug, DOX), UV-vis spectroscopic analysis was conducted. The optical properties of metal NPs are based on the localized surface plasmon resonance (LSPR) principle which is governed by the collective excitation of the conduction electrons due to irradiation by light in the visible and near-IR regions of the electromagnetic spectrum (Harris *et al.,* 2012).

Figure 4.2.1 and figure 4.2.2 show the UV-vis absorbance peaks produced by the NPs and DOX-loaded NCs from the chemical and biosynthesis methods respectively. The bands of absorption at 260 nm and 320 nm in figure 4.2.1 (a), and the ones at 263 nm and 320 nm in figure 4.2.2 (b) are presented as saddle and narrow peaks, suggesting the creation of the bimetallic silver and selenium NPs, given that Se NPs are recognized to peak between 200 – 300 nm and Ag NPs are reported to peak between 390 – 490 nm (Alwhibi *et al.*, 2018; Alagesan and Venugopal, 2019). The slight shift in the F-SeAg NPs first peak

absorbance compared to the SeAg NPs is possibly caused by the presence of fenugreek seed extract bio-compounds acting as stabilizing agents. The red shift in the absorbance to 350 nm (figure 4.2.1 b) and 348 nm (figure 4.2.2 c) suggested a change in surface electrons/optical properties brought about by the attachments of Ch-PEG, indicating the formation of SeAgChPEG NPs and F- SeAgChPEG NPs respectively. A comparable band shifting absorption following the functionalization of these NPs is observed with the creation of SeAgChPEGFA NPs at 445 nm (figure 4.2.1 c) and F-SeAgChPEGFA NPs at 448 nm (figure 4.2.2 d), confirming the attachment of FA as previously reported (Yang *et al.*, 2018). The known LSPR peak of DOX is around 480 nm and 490 nm (Liang *et al.*, 2018). Therefore, the LPSR peaks at 475 nm (figure 4.2.1 d) and 478 nm (figure 4.2.2 e) suggested the formation of the SeAgChPEGFA@DOX NCs and F-SeAgChPEGFA@DOX NCs respectively. The findings relate to literature (Nayak *et al.*, 2016; Paszkiewicz *et al.*, 2016; Maney and Singh, 2017; Zohreh *et al.,* 2022). The UV spectra of FA, Ch, PEG, and DOX are shown in figure A1, appendix.

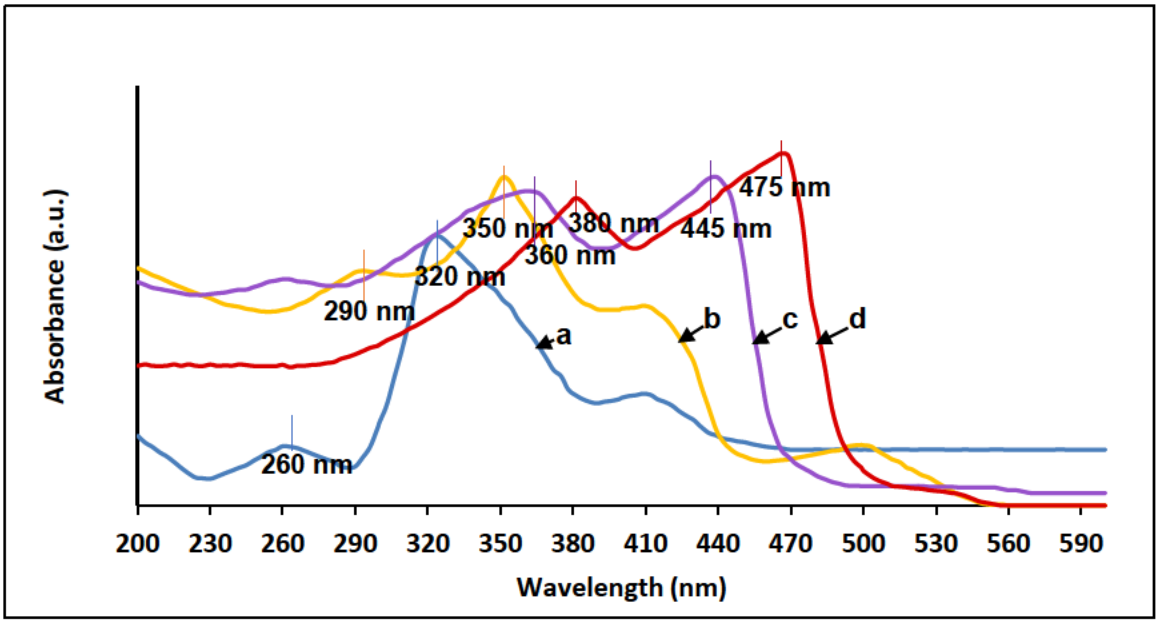

Figure 4.2.1: UV-vis spectra of the chemically synthesized (a) SeAg NPs, (b) SeAgChPEG NPs, (c) SeAgChPEGFA NPs, and (d) SeAgChPEGFA@DOX NCs.

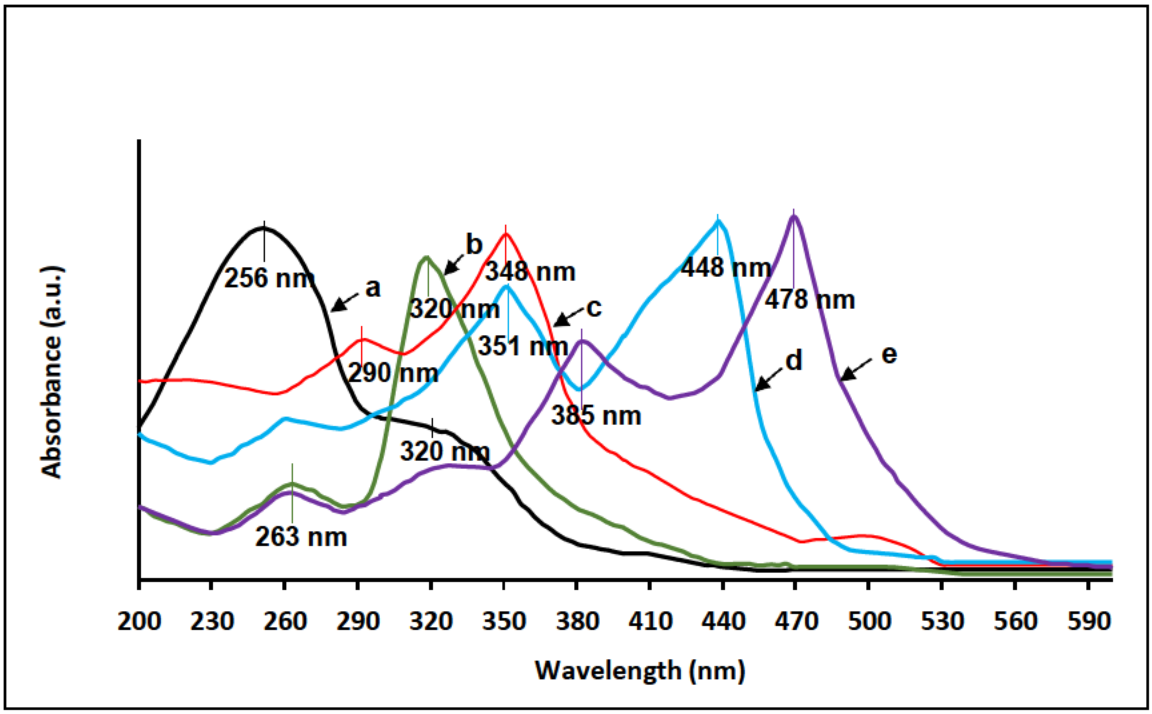

Figure 4.2.2: UV-vis spectra of (a) Fenugreek extract (F), (b) F-SeAg NPs, (c) F-SeAgChPEG NPs, (d) F-SeAgChPEGFA NPs, and (e) F-SeAgChPEGFA@DOX NCs.

4.1.3 FTIR Spectroscopic Analysis

FTIR analysis was conducted to further verify the positive formulation and functionalization of NPs/NCs, by identifying the functional groups that are on the surface of the NPs/NCs (Nayak *et al.*, 2016). Figure 4.3.1 and figure 4.3.2 show the spectra of the chemically and biosynthesized NPs and their NCs. The SeAg NPs and F-SeAg NPs spectra (figure 4.3.1 a and 4.3.2 a) show characteristic peaks at 2968 cm^{-1} and 2972 cm^{-1} corresponding to C-H stretch alkynes, the peaks at 1652 cm^{-1} and 1644 cm^{-1} corresponded to N-O asymmetric stretch nitro compounds; and the peaks at 1529 cm^{-1} and 1537 cm^{-1} corresponding to hydroxyl groups (O-H). These findings are similar to previous reports (Amany *et al.,* 2012; Ruiz-Fresneda *et al.,* 2020).

In addition, the fenugreek seed extract spectrum in figure A2 has some bands similar to the spectrum of F-SeAg NPs with slight band shifting and reduction in intensity. For example, the typical bands such as a hydroxyl group (O-H) and amine (N-H) at 3324 cm^{-1}, and a methylene (CH_2) group at 1496 cm^{-1} seen in figure A2 appear in the extract-reduced F-SeAg NPs spectrum (figure 4.3.2 a). These biomolecules are known to be involved in the reduction of metal ions to metal NPs (Ahmad *et al.,* 2011; Annamalai *et al.,* 2013; Ramamurthy *et al*., 2013).

Moreover, the attachment of Ch-PEG onto the NPs as seen in figure 4.3.1 b and figure 4.3.2 b, resulted in alcohol bendings (O-H) at 2877 cm^{-1} and 2875 cm^{-1}, respectively; distinct carbonyl (C =O) groups at 1662 cm^{-1} and 1642 cm^{-1}, respectively; aldehyde stretchings (C-O-H) at 1558 cm^{-1} and 1541 - 1531 cm^{-1}, respectively; and lastly, out-of-plane bending of an amine (NH) appearing at 817 cm^{-1} and 855 cm^{-1}, respectively. These findings validated the successful conjugation of the polymers via the amide bonding which resulted in the formation of SeAgChPEG NPs and F-SeAgChPEG NPs, respectively (Wang *et al.*, 2018; Daniels and Singh, 2019; Akinyelu and Singh, 2019).

Following the functionalization of the NPs with FA, distinct carbonyl bendings (C=O) at 1670 cm^{-1} and 1649 cm^{-1}, as well as bands of a phenyl ring at 1341 cm^{-1} and pterin ring at 1207 cm^{-1}were respectively observed (figure 4.3.1 c and figure 4.3.2 c), which confirms

FA attachment to the Ch-PEG through amide bonds (Akinyelu and Singh, 2019). The spectrum of the SeAgChPEG@DOX NCs (figure 4.3.1 d) and that of F- SeAgChPEGFA@DOX NCs (figure 4.3.2 d) respectively showed hydrocarbon groups (C-H) at 2943 $cm^{-1}$and 2972 cm^{-1}; amino groups (NH_2) at 1674 cm^{-1} and 1680 cm^{-1}; and ether linkages (C-O-C) at 1533 cm^{-1} and 1534 cm^{-1}, confirming DOX conjugation. Data of the functionalized NPs/NCs corresponds to the FTIR spectra of DOX, FA, PEG, and Ch represented in figure A2 (Liang *et al.*, 2018; Wang *et al.*, 2018).

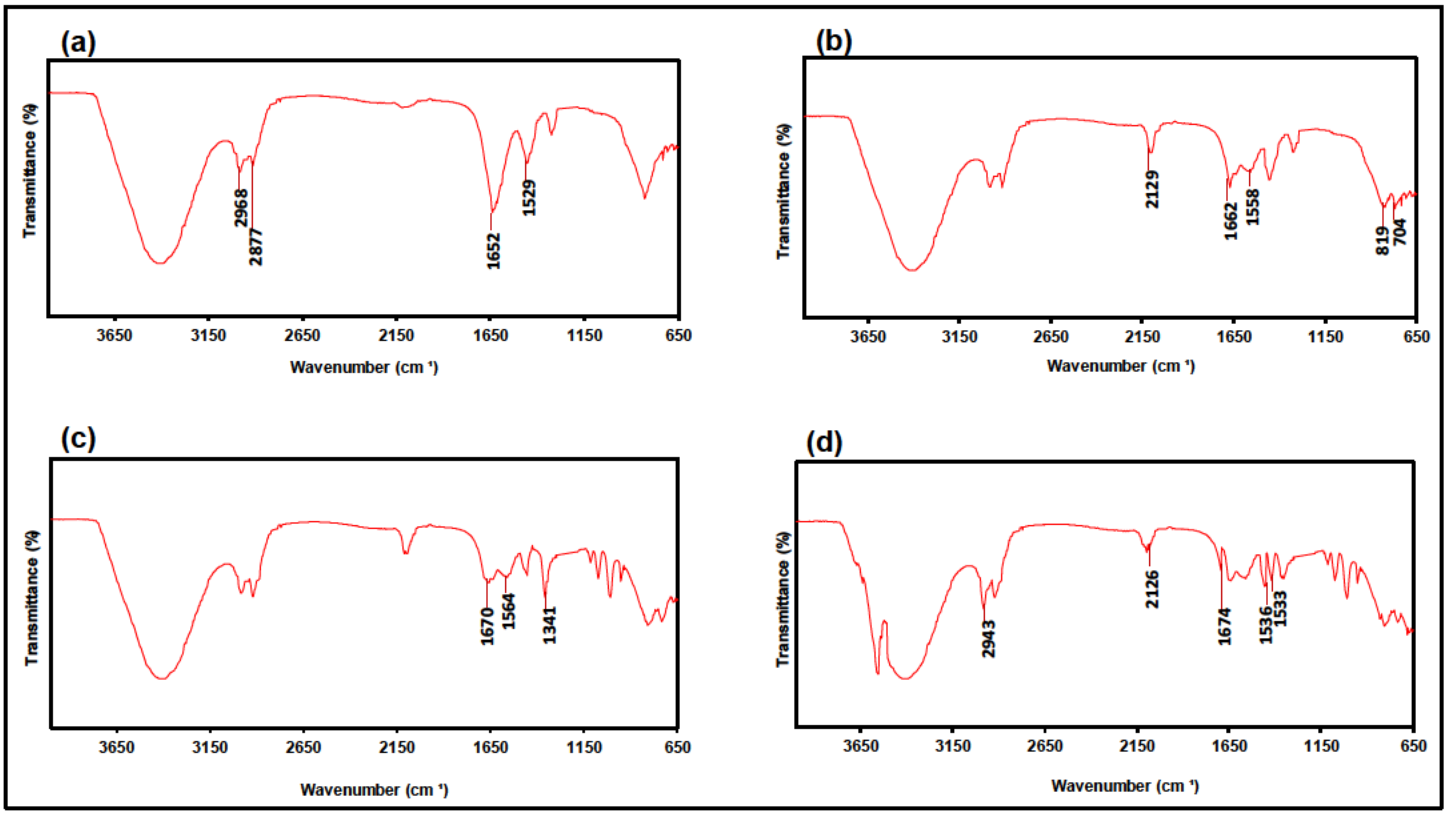

Figure 4.3.1 (a – d): FTIR spectra of the chemically synthesized (a) SeAg NPs, (b) SeAgChPEG NPs, (c) SeAgChPEGFA NPs, and (d) SeAgChPEGFA@DOX NCs.

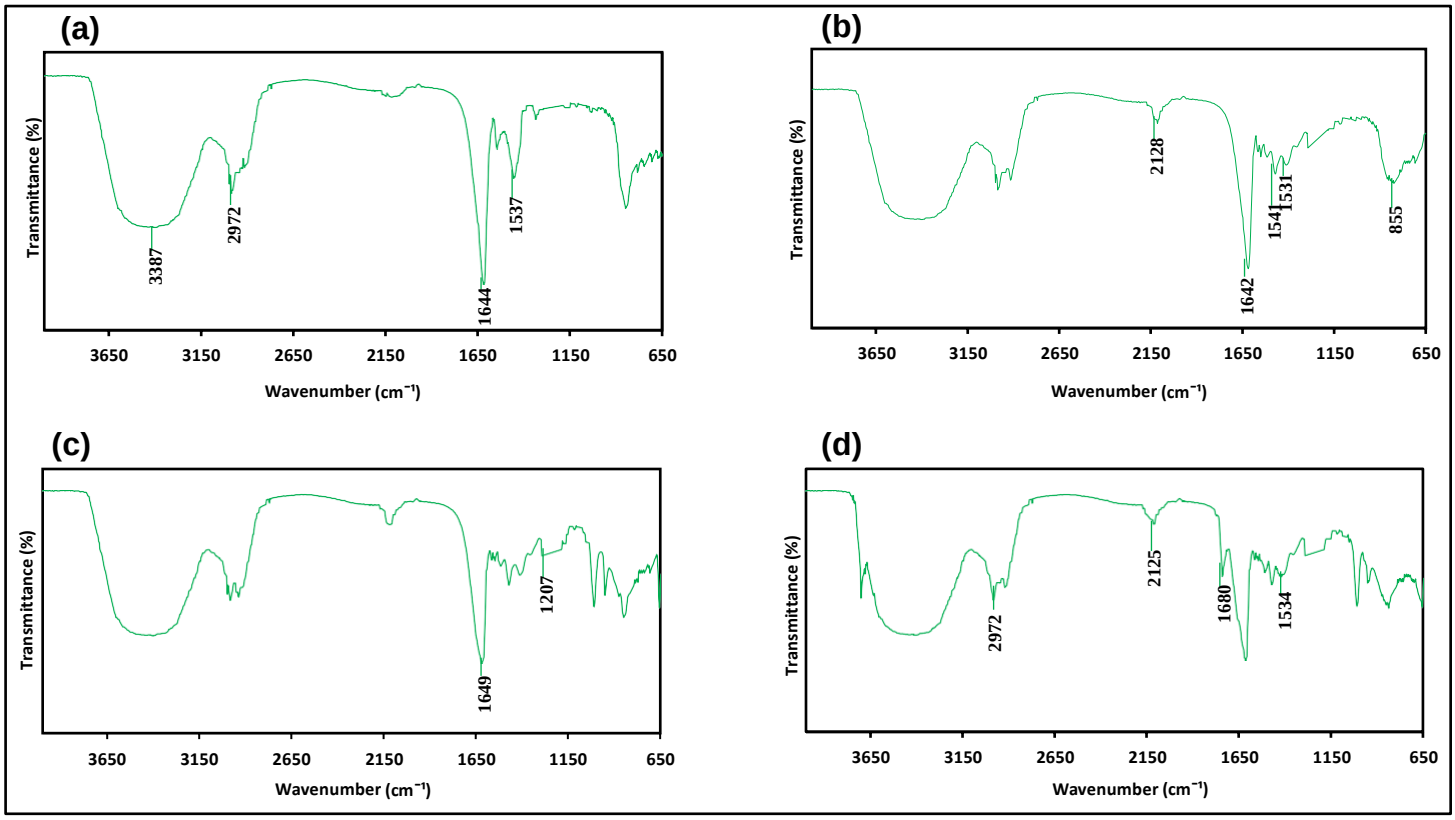

Figure 4.3.2 (a – d): FTIR spectra of the biosynthesized (a) F- SeAg NPs, (b) F-SeAgChPEG NPs, (c) F-SeAgChPEGFA NPs, and (d) F-SeAgChPEGFA@DOX NCs.

4.1.4 Morphology, Size, and *Zeta* Potential Analysis

4.1.4.1 Morphology Analysis

The morphology, size, and surface charge of the NPs are crucial elements influencing both the cellular uptake and the pharmacokinetics of the NPs in drug-delivery studies (Truong *et al.,* 2015). The size and charge of NPs, particularly, can strongly influence the cellular interaction and internalization, and the bio-distribution/dispersity of the therapeutic drug, and hence influence the overall therapeutic efficacy of the drug (Ridolfo *et al.,* 2020).

Figure 4.4.1 and figure 4.4.2 shows TEM micrographs of the chemically and the biosynthesized NPs/NCs respectively. The NPs appeared spherical and uniformly distributed (figure 4.4.1 a-c and figure 4.4.2 a-c), while the NCs appeared as spherical

clusters (figure 4.4.1 d and figure 4.4.2 d). Spherical Se and Ag NPs have been studied and their effectiveness has been reported in previous literature (Shkhair *et al.,* 2018; Zhou *et al.,*2021).

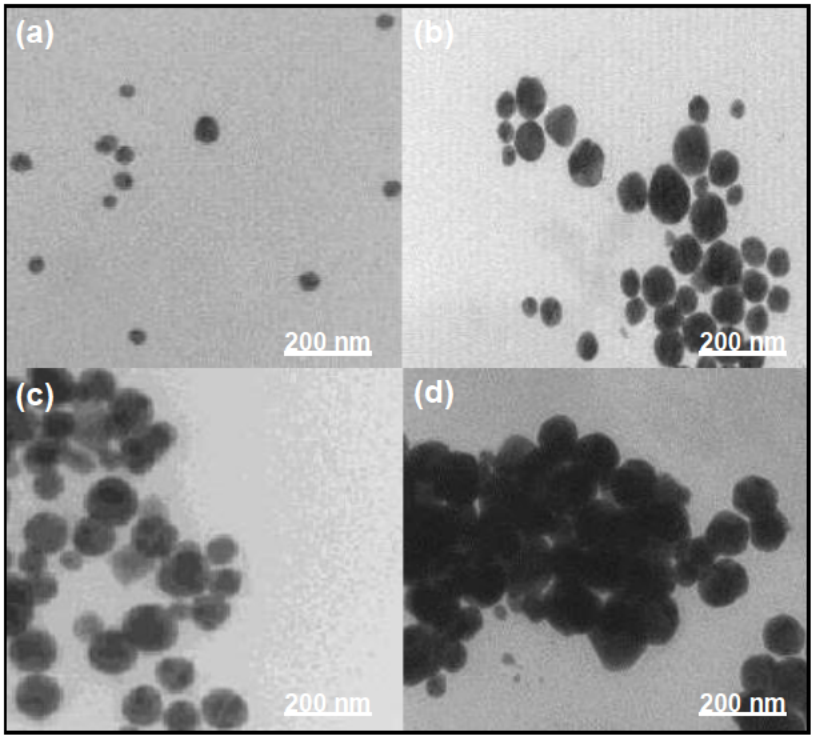

Figure 4.4.1 (a – d): TEM micrographs of the chemically synthesized (a) SeAg NPs, (b) SeAgChPEG NPs, (c) SeAgChPEGFA NPs, and (d) SeAgChPEGFA@DOX NCs. Scale bars: 200 nm.

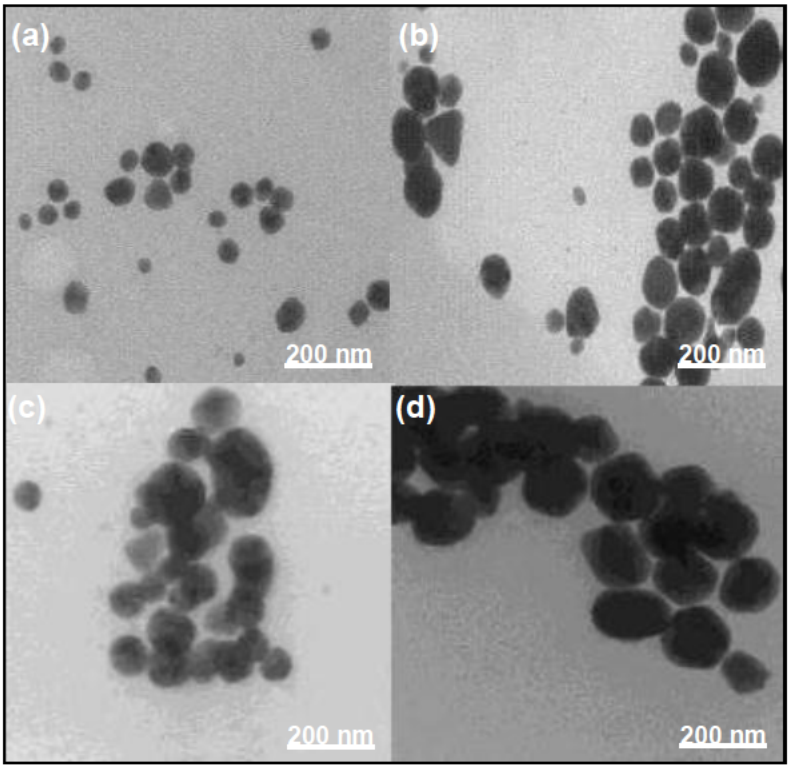

Figure 4.4.2 (a – d): TEM micrographs of the biosynthesized (a) F-SeAg NPs, (b) F-SeAgChPEG NPs, (c) F-SeAgChPEGFA NPs and (d) F-SeAgChPEGFA@DOX NCs. Scale bars: 200 nm.

4.1.4.2 Size and Zeta Potential Analysis

The NPs size and *zeta* potential significantly influence the efficacy of the drug-delivery system. According to literature, the size of the NPs plays an important role in the potential delivery of bioactive materials to the cancerous sites because of the numerous capabilities of nanocarriers such as the chemo-physical serum stability, ability to carry a specific amountof a drug, stabilizing polymers and targeting moieties have been considered as size- dependent characteristics (Chalati *et al.,* 2011; Azadpour *et al.,* 2022). Furthermore, studies have reported that NPs with sizes larger than 200 nm induce the activation of the complement system, resulting in their rapid elimination from the bloodstream and accumulation in the spleen and liver, compared to those under 200 nm which display decreased rates of clearance and consequently reach an extended circulation time (de Barros *et al.,* 2012; Kulkarni and Feng, 2013).

Table 1 shows the sizes of the chemically and biosynthesized NPs/NCs as determined by the dynamic light scattering analysis from the ζ sizer. The size of the chemically synthesized NPs ranged between 103.5 ±0.3 nm – 133.1 ± 0.1 nm, while that of their NCs was 154.9 ± 0.4 nm. On the other hand, the biosynthesized NPs sizes ranged between 105.2 ± 0.2 nm – 138.8 ± 0.2 nm, while their NCs were 158.7 ± 1.1 nm. The size differences observed between the NPs are due to surface functionalization of the NPs by copolymers (Ch and PEG) and a targeting ligand (FA) as previously reported (Maiyo and Singh, 2017; Agarwal *et al.*, 2018; Maiyo and Singh, 2020). The attachment/encapsulationof DOX onto the surface of the NPs also brought about an increase in the sizes of the resulting NCs. Overall, the NPs/NCs sizes obtained fall within the size required foreffective drug delivery, suggesting that they are suitable drug-delivery modalities (de Barros *et al.,* 2012; Kulkarni and Feng, 2013).

Furthermore, the colloidal stability of NPs which is confirmed by their *zeta* potential is fundamental in controlling their application in biomedicine, more especially in drug delivery (Akinyelu and Singh, 2019). *Zeta* (ζ) potential is described as the net electrical charge between the surface of NPs and the surrounding solvent, which in turn signifies the NP colloidal dispersions' stability (Clogston and Patri, 2011). Nanoparticles exhibiting high ζ potentials (positive or negative), with a charge more than 30 mV or less than -30 mV are supposedly electrically stable, whereas those with low ζ potentials less than 30 mV and more than -30, are supposedly electrically unstable, therefore have a tendency to agglomerate upon administration (Clogston and Patri, 2011; De Trizio *et al.*, 2017), which hinders their circulation time, resulting in pre-mature bio-system clearance.

The ζ potential measurements of NPs and NCs as determined by a *Zeta* sizer are presented in table 1 and figures (A3 and A4, appendix). The ζ potential measurements of chemically synthesized NPs ranged from -26.2 ± 0.4 mV to 58.3 ± 0.8 mV, and that of theirNCs counterparts was 53.1 ± 2.3 mV. While those of biosynthesized NPs ranged from -34.4 ± 0.9 mV to 61.1 ± 1.1 mV, and that of their NCs was 57.4 ± 1.9 mV. It was observed that the inclusion of copolymers on the NPs caused an alteration in ζ potential charges

from negative to positive, validating the attachment of a positively charged Ch onto the negatively charged surface of the NPs. This corresponds with previous studies (Chen *et al.*, 2015; Akinyelu and Singh, 2019). The addition of FA resulted in a slight decrease in the ζ potentials of the Ch-PEG tagged NPs. This can be attributed to the reduced positive charges on the copolymer-capped NPs given that some Ch charges are involved in the attachment of FA (Angelopoulou *et al.*, 2019).

Table 1. Size distribution, and *zeta* potential of NPs and their NCs. Data presented as mean diameter or *zeta* potential ± standard deviation (SD) (n=3).

NPs/DOX-loaded NCs	Size (nm)	ζ Potential (mV)	NP: DOX ($^{w/}_{w}$) ratio
SeAg	103.5 ± 0.3	-26 .2 ± 0.4	-
SeAgChPEG	130.5 ± 0.1	59.8 ± 1.4	-
SeAgChPEGFA	133.1 ± 0.1	58.3 ± 0.8	-
SeAgChPEGFA@DOX	154.9 ± 0.4	53.1 ± 2.3	1:0.8
F- SeAg	105.2 ± 0.2	-34.4 ± 0.9	-
F- SeAgChPEG	136.4 ± 0.4	62.4 ± 1.0	-
F- SeAgChPEGFA	138.8 ± 0.2	61.1 ± 1.1	-
F-SeAgChPEGFA@DOX	158.7 ± 1.1	57.4 ± 1.9	1:0.9

Overall, both the chemically synthesized and biosynthesized BMNPs displayed good stabilities (58.3 ± 0.8 mV and 61.1 ± 1.1 mV respectively), with the biosynthesized, F-SeAgChPEGFA NPs (61.1 ± 1.2 mV) presenting higher stability. This could be due to the stabilization of these NPs by biomolecules such as the O-H groups (flavonoids, polysaccharides, polyphenols) present in the aqueous fenugreek seeds extract in addition to the coating with Ch and PEG (Huang and Yang, 2004; Gillich *et al.,* 2013; Deshmukh *et al.,*2019; Oladipo *et al.,* 2020). Although the attachment of DOX onto the chemically and biosynthesized NPs slightly reduced the ζ potentials (53.1 ± 2.3 mV and 57.4 ± 1.9 mV), a relatively good stability was still maintained. This could be due to the reduction in the number of the amine groups of Ch because of their additional participation in the encapsulation of DOX (Maney and Singh, 2019). In general, the findings suggested that both methods of synthesis yielded effective bimetallic NCs with the F-SeAgChPEGFA@DOX NCs demonstrating slightly greater physiological characteristics vital

for improved cellular uptake, and increased biocompatibility for enhanced drug therapeutic efficiency.

4.1.5 Encapsulation Efficiency (EE%) and Drug loading (DL%) Percentage Analysis

Determining the amount of drug loaded onto NPs and the efficiency of its encapsulation are two important properties that must be evaluated because they influence the effectiveness of the delivery systems (Judefeind and de Villiers, 2009). In addition, the amount of drug encapsulated also determines the functioning of the drug-delivery systems because it influences the rate and degree of drug release from the system. Therefore, to ascertain the mass ratio of drug-to-drug-loaded NPs to the encapsulated drug (DL%) and the percentage of the drug that is successfully entrapped into the DOX-loaded NCs (EE%) binding evaluations were done.

The sedimentation of NPs through centrifugation is an elementary, dependable, and precise method to remove the unbound drug particles. NPs that are drug-bound sediment at different speeds based on size, mass, and viscosity (Maney and Singh, 2017). The DOX-loaded NCs were generally of higher size and mass, and subsequently formed pellets, whereas the unbound DOX remained in the supernatant. Upon UV-vis spectroscopy and calculations, the EE% and DL% of the SeAgChPEGFA@DOX NCs were found to be 84% and 26%, respectively; while those of the F-SeAgChPEGFA@DOX NCs were found to be 87% and 22%, respectively (table A1). The higher EE% detected with F-SeAgChPEGFA@DOX NCs can be credited to their greater ζ potential (57.4 ± 1.9 mV), indicating the relation between the ζ potential and the resultant EE%. The low DL% in contrast can be credited to the density of the drug-loaded NCs (Maney and Singh, 2019). These findings corroborated previously reported studies (Xia *et al.*, 2018; Maney and Singh, 2019).

4.1.6 *In Vitro* Release Analysis

The *in vitro* kinetics of NPs provide important information on their ability to facilitate and modify drug release in cancer cells (Yu *et al.*, 2020). The microenvironment of cancer cells is known to be acidic with a pH range between pH 4 and 6, owing to the metabolic abnormalities, which result in the influx of acidic metabolites into the

lysosomes/endosomes (Xia *et al.*, 2018; Angelopoulou *et al.*, 2019). The *in vitro* drug release profiles of the chemically synthesized SeAgChPEGFA@DOX NCs (figure 4.5 a) and biosynthesized F- SeAgChPEGFA@DOX NCs (figure 4.5 b) were investigated in PBS solutions of pH 4.4, 5.4, and 7.4 at 37 °C for 72 hours using a dialysis procedure. These buffer pHs created a normal physiological environment and induced tumor cell microenvironments (Xia *et al.*, 2018). The DOX release profiles from both NCs (figure 4.5 a-b) were acid-dependent and displayed a two-phase release behavior, primarily starting with a burst in the initial 24 hours, followed by a slow constant release of DOX in a plateau phase for the remaining hours. The findings corroborate with previous studies (Du *et al.*, 2014; Yu *et al.*, 2014; Xia*et al.*, 2018; Maney and Singh, 2019; Xia *et al.*, 2020). The preliminary drug burst releasecan be attributed to the release of the drug on the surface of the NPs, while the plateau phase can be credited to the slow release of the drug encapsulated within the NPs (Rafiei and Haddadi, 2017).

At pH 4.4, both the SeAgChPEGFA@DOX NCs and F- SeAgChPEGFA@DOX NCs exhibited substantially quicker DOX release levels of up to 83% and 88%, respectively, at 72 hours, whereas at the physiological pH 7.4, the release levels were consistently slower and up to 31% and 26%, respectively. The efficient DOX release in an acidic environment can be accredited to the diminished surface charges on both NPs owing to PEG shielding, which reduces the interaction between DOX and the NPs (Xia *et al.*, 2020; Mbatha and Singh, 2019). The higher release rate prompted by both DOX-loaded NCs suggested that upon transfection into the cells, these would release the DOX faster from the lysosome, thus avoiding degradation and enhancing the drug's therapeutic efficiency (Mbatha and Singh, 2019; Xia *et al.*, 2020). Also, the acid-dependent DOX release characteristic is essential for anticancer drug-delivery vectors given that most cancer cells are more acidic compared to healthy cells (Xia *et al.*, 2018). Overall, these results impose the perception that the biosynthesized F- SeAgChPEGFA@DOX NCs retained exceptional drug-carrying and releasing capabilities over the chemically synthesized SeAgChPEGFA@DOX NCs counterparts, hence making them better delivery modalities.

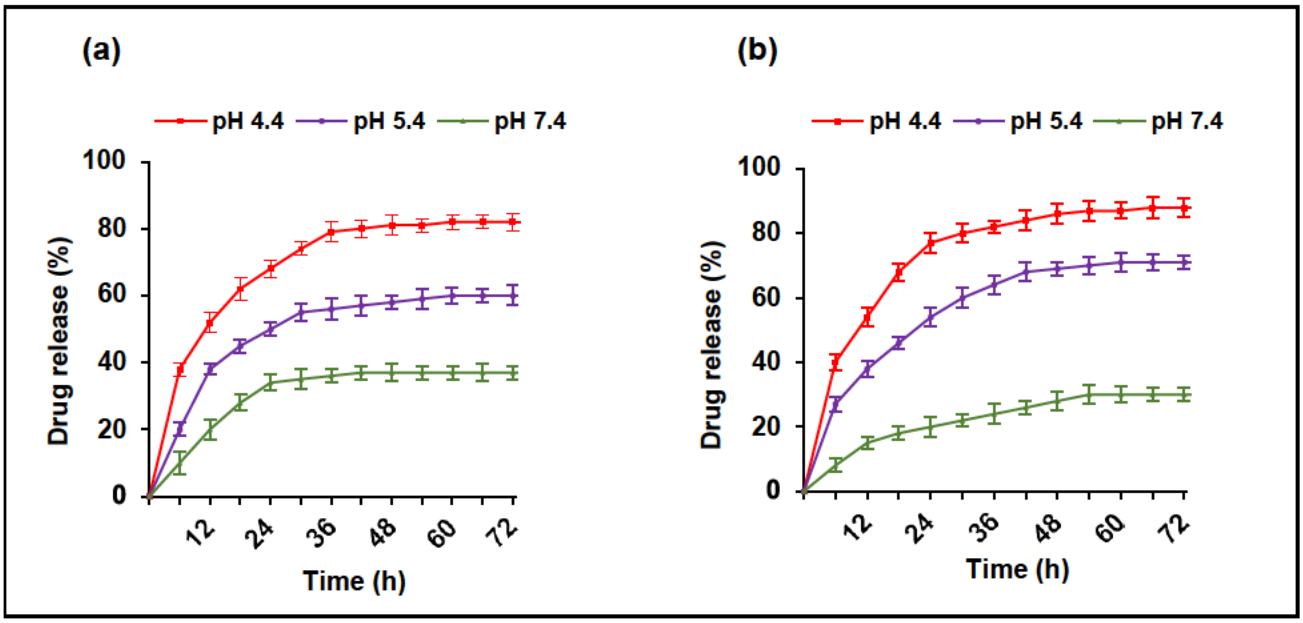

Figure 4.5 (a – b): *In vitro* release analysis of (a) SeAgChPEGFA@DOX NCs and (b) F-SeAgChPEGFA@DOX NCs at pH 4.4, 5.4, and 7.4 in 72 hours.

4.1.7 MTT Analysis

The effective use of NPs in cancer therapy applications, particularly, in drug delivery, primarily relies on their toxicity, therefore, determining the NPs cytotoxic profile is important (Maney and Singh, 2017). For this investigation, the MTT assay was undertaken to assess the cytotoxicity profiles of the SeAgChPEGFA NPs, F-SeAgChPEGFA NPs, the DOX-loaded NCs, and free DOX, against HEK293 non-cancer and HeLa cancer cells. This assay is established by the principle that only viable cells with functional mitochondrial dehydrogenase enzymes can reduce the yellow soluble tetrazolium salt topurple insoluble formazan which can be measured spectroscopically, where the absorbance values are directly proportional to the number of live cells (figure 4.6) (Patra*et al.,* 2018). The results are presented in figure 4.6.1, figure 4.6.2, and figure A5 and A6 in the form of half maximal inhibitory concentration (IC_{50}) values. In general, an IC_{50} valueexpresses the concentration of the drug/NPs required to eradicate 50% of the tested cells.Therefore, lower IC_{50} values suggest the potency and efficiency of the NPs (Berrouet *et al.,* 2020).

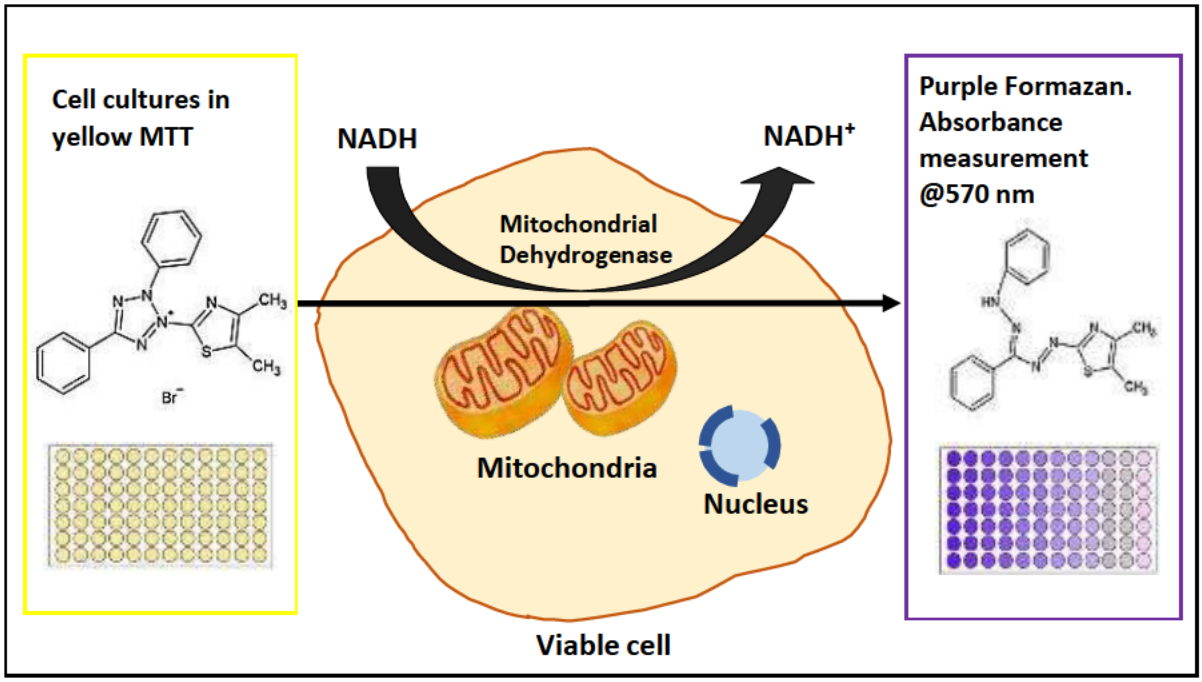

Figure 4.6: An illustration of the conversion of water-soluble tetrazolium salt (yellow) into a water-insoluble formazan product (purple colour) (adapted from Ligasová and Koberna, 2021).

The HeLa cancer cells and HEK293 non-cancer cells were treated with several concentrations from 5 – 25 µg/ml of the drug-free SeAgChPEGFA NPs, F-SeAgChPEGFA NPs, SeAgChPEGFA@DOX-loaded NCs, F-SeAgChPEGFA@DOX-loaded NCs and free DOX (figure 4.6.1 and figure 4.6.2). The findings show that the viability of the cells was cell-specific and dependent on the concentration. Figure 4.6.1 a-b shows that upon treatment of the cells (HeLa and HEK293) with both the drug-free SeAgChPEGFA NPs and F-SeAgChPEGFA NPs, no significant cell inhibition was observed as demonstrated by the cell viabilities ≥ 85% across tested concentrations. This suggested the biocompatibility and safety of both NPs, particularly the biosynthesized F-SeAgChPEGFA NPs. This couldbe attributed to the biodegradable, biocompatible, and non-toxic/benign biomolecules used to formulate these NPs (Collado-González *et al.,* 2017; Wang *et al.,* 2018).

Moreover, figure 4.6.2 a-b, showed that there was a systematic decrease in cell viability with increasing DOX concentrations/dose upon treatment of the tested cells with SeAgChPEGFA@DOX-loaded NCs and F-SeAgChPEGFA@DOX-loaded NCs. Wherein, significant ($p < 0.001$) cell growth inhibitions were observed at the DOX concentration of

25 µg/ml with cell viabilities of 35% and 33% respectively. Herein, free DOX also had notable cell growth inhibition on the cancer HeLa cells with cell viability of 40% at 25 µg/ml. This could be attributable to its capability to instantly induce its effects upon entering the cells. Nonetheless, this instant effect is inadequate for systemic use because repetitive use induces drug resistance and undesirable side effects. The higher growth inhibition effect demonstrated by the DOX- loaded NCs compared to the drug-free NPs and free DOX can be attributed to a combination of factors including (a) the synergistic effect of Ch-PEG coated Se-Ag core- shell and the loaded DOX (Siwowska *et al.,* 2017), (b) the increased cellular uptake due tothe FA ligand which has an affinity for the folate receptors overexpressed by these cells (Scaranti *et al.,* 2020), (c) the higher stability (smaller size, and higher ζ potential) which favours faster cellular uptake, and longer intracellular circulation, (d) the higher drug encapsulation efficiency (84% and 87%), and (e) the faster, and controlled drug release efficiency. Furthermore, the lower IC_{50} values of both DOX-loaded NCs (figure A6), particularly that of F-SeAgChPEGFA@DOX NCs (16.70 µg/ml), show that these NCs are effective at low concentrations, and thus may show subordinate systemic toxicity when administered *in vivo*, in comparison to free DOX (19.67 µg/ml) (Maney and Singh, 2019; Fernández-Villa *et al.,* 2018).

The treatment of non-cancer HEK293 cells with the DOX-loaded NCs showed neglectable cell growth inhibitory effects as demonstrated by cell viabilities > 85%. On the other hand, free DOX showed some degree of inhibition, though the effect was not profound with cell viabilities > 69%. Overall, the results suggested that both the drug-free NPs and DOX-loaded NCs did not induce harmful effects on the normal cells, signifying their biocompatibility and safety, hence the slightly detected cytotoxicity induced by the DOX-loaded NCs compared to the drug-free NPs can be attributed to the conjugated anticancer drug, DOX (Xu *et al*., 2015; Liu *et al*., 2019; Maney and Singh, 2019).

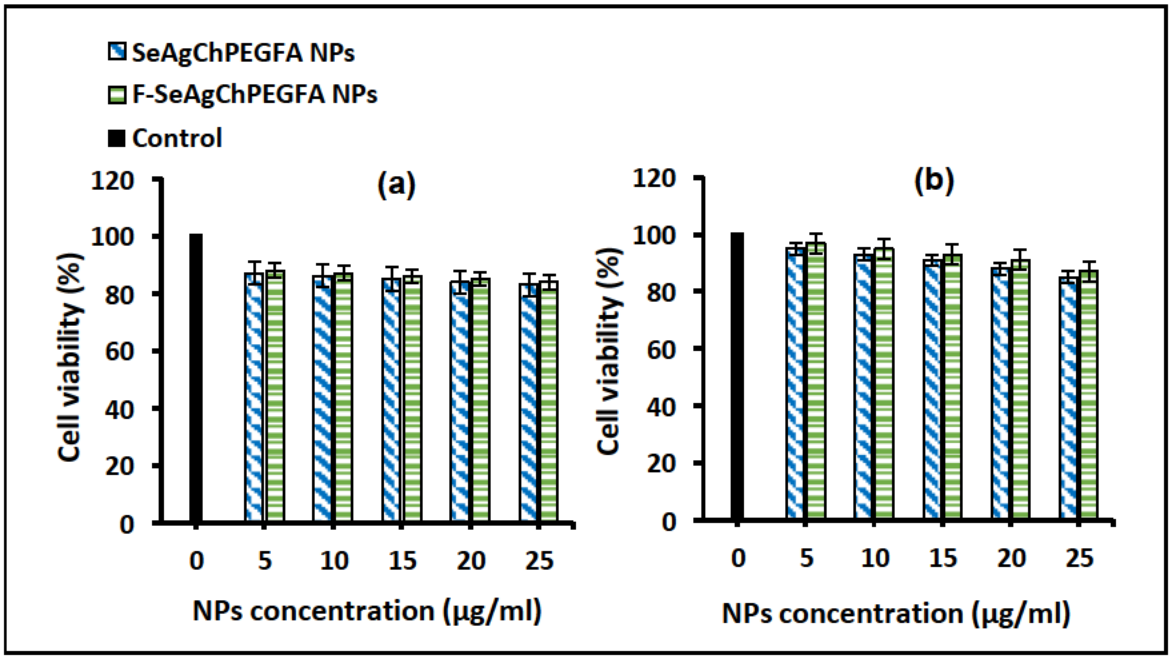

Figure 4.6.1 (a – b): MTT cell viability after treatment with SeAgChPEGFA NPs, and F-SeAgChPEGFA NPs in (a) HeLa, (b) HEK293 cells. The data is presented as means ± SD (n=3). Control: untreated cells. **p*<0.05, ***p*<0.01, ****p*<0.001 vs control.

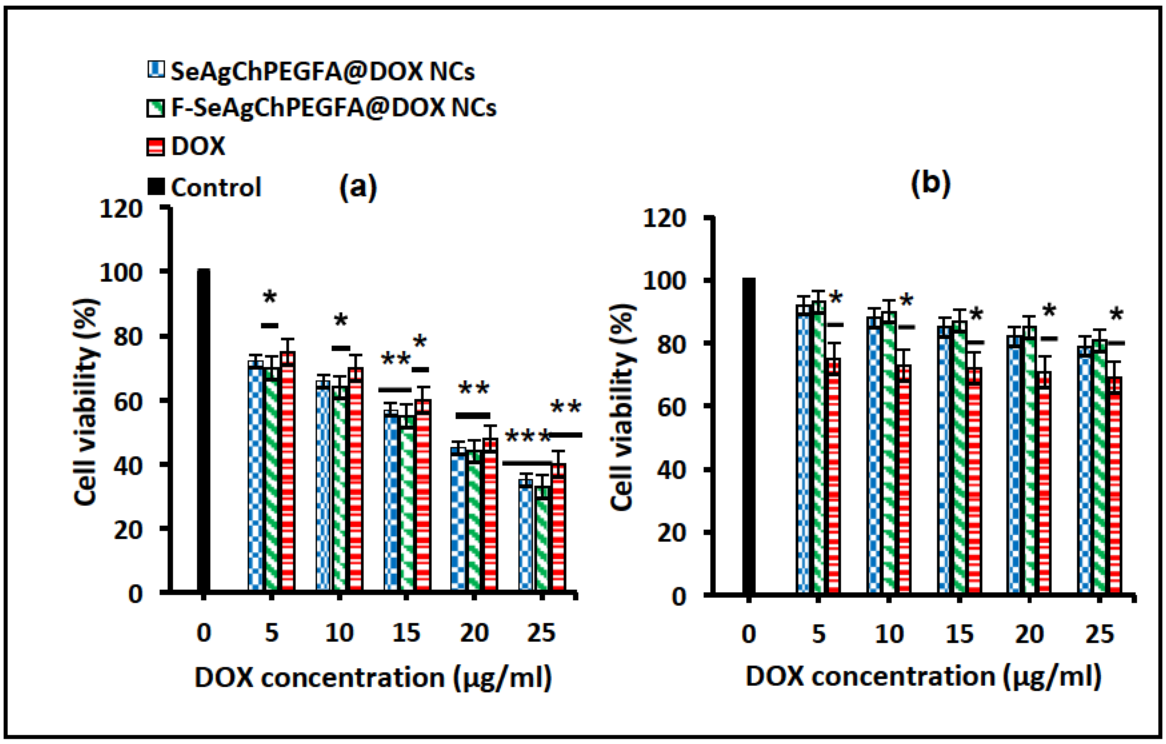

Figure 4.6.2 (a – b): MTT cell viability after treatment with SeAgChPEGFA@DOX NCs, F-SeAgChPEGFA@DOX NCs, and free DOX in (a) HeLa, (b) HEK293 cells. The data is presented as means ± SD (n=3). Control: untreated cells. *p<0.05, **p<0.01, ***p<0.001 vs control.

4.1.8 Anticancer Analysis

Apoptosis, better known as programmed cell death, is an important mechanism the cells use to regulate homeostasis between cell growth and death (Mbatha and Singh, 2019; Maiyo and Singh, 2020). Improper regulation of this mechanism leads to the development of cancer; hence, its utilization is of significance in anticancer drug discovery (Maney and Singh, 2019). During apoptosis, the cell undergoes a sequence of structural changes such as shrinkage of the cell, fragmentation into membrane-bound apoptotic bodies, and rapid phagocytosis by neighbouring cells; classified into early apoptosis (EA), and late apoptosis (LA) (Saraste and Pulkki, 2000).

The apoptosis assay used to evaluate the apoptotic profiles of the NPs, DOX-loaded NCs, and DOX uses AO/ETBR dual staining dyes, which allows the microscopic assessment of these variations in the cell membrane and the nucleus of cells in cell structure, by

differentiating the normal cells, and those in different stages of apoptosis. The AO stain is usually up taken by both viable and early apoptotic cells, whereas the ETBR dye is selectively taken up by the non-viable cells with compromised membrane integrity and as a result causes their nucleus to fluoresce bright orange (Liu *et al.,* 2015, Maiyo and Singh, 2019). Therefore, EA cells appear bright green to yellow with a granular or crescent-shaped nucleus and LA cells display an asymmetrical nucleus with an orange colour.

The microscopic fluorescent images of the cancer cells (HeLa) and non-cancer cells (HEK293) untreated and those treated with NPs, their DOX-loaded NCs and free DOX at 25µg/ml are presented in figure 4.7 a-b; and their apoptotic indices (AI) are shown in table 2. Untreated cells appeared green, indicative of viable cells (L) and all the remedied cells exhibited different levels of programmed cell death with EA depicted as mustard/yellow and LA as a dark shade of orange symbolic of non-viable cells (Xie *et al.*, 2017). Treatment of HeLa cancer cells with the SeAgChPEGFA@DOX and F-SeAgChPEGFA@DOX NCs significantly suppressed the cancer cells' growth (AI = 0.742 ± 0.051 and 0.750 ± 0.034, respectively) compared to free DOX (AI = 0.570 ± 0.030). This can be attributed to the controlled drug release capability presented by the respective NPs as previously determined in section 4.1.6 (figure 4.5). Furthermore, when compared to the drug-free NPs (AI = 0.056 ± 0.001 and 0.062 ± 0.002 respectively), both DOX-loaded NCs were more effective in suppressing tumor growth, confirming their improved antitumor activity. The treatment of HEK293 non-cancer cells with the drug-free NPs and DOX-Loaded NCs showed negatable apoptosis activity (AI = 0.001 ± 0.0002 – 0.003 ± 0.0002), signifying the biocompatibility and safety of these nano-delivery systems. Overall, these results are consistent with those established in the MTT study.

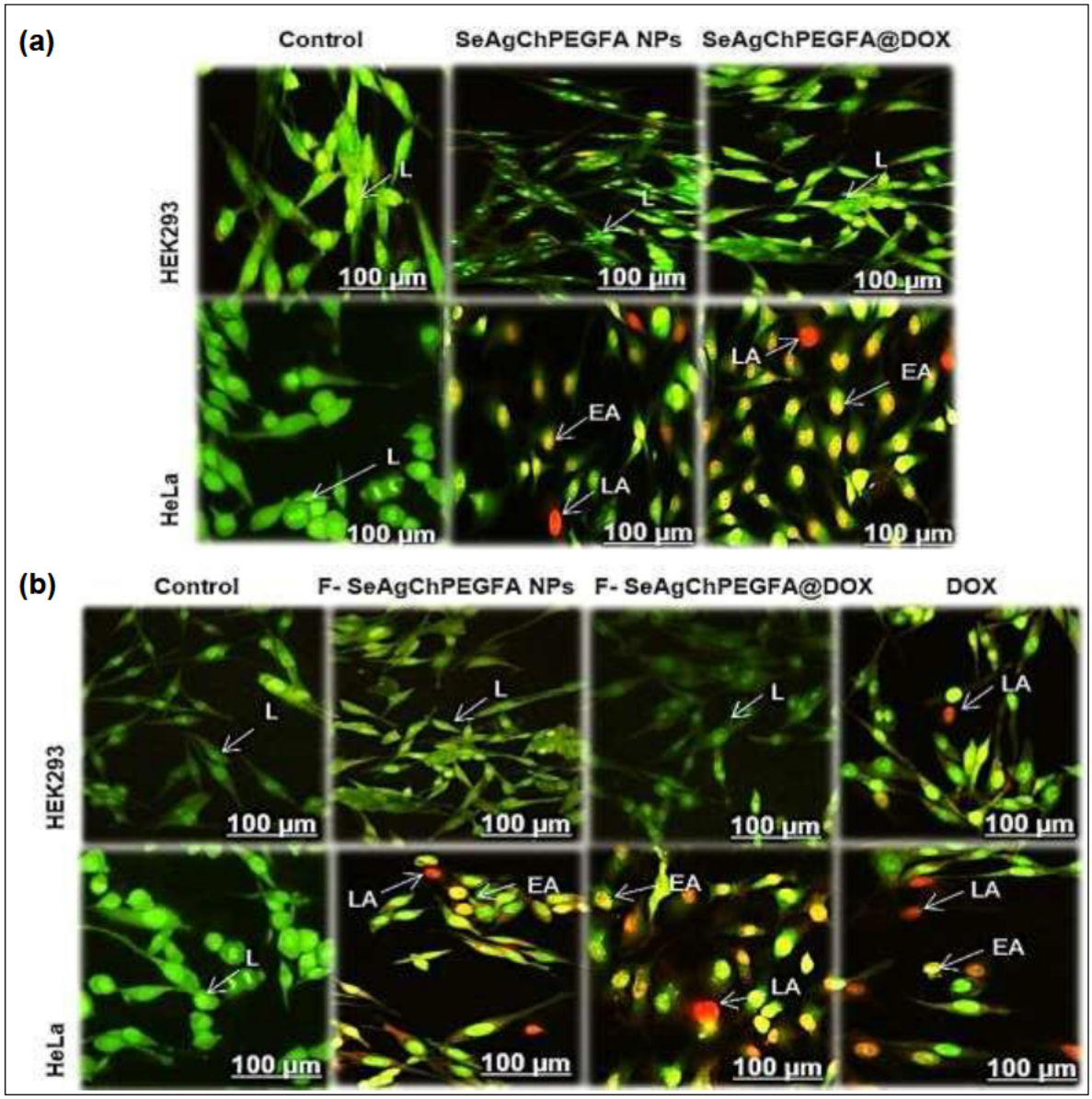

Figure 4.7 (a – b): Fluorescence images of HeLa, and HEK293 cells after treatment with SeAgChPEGFA NPs, F-SeAgChPEGFA NPs, SeAgChPEGFA@DOX NCs, F-SeAgChPEGFA@DOX NCs, and free DOX showing apoptosis induction. Green = live (L) cells, yellow = early apoptotic (EA) cells, and orange = late apoptotic (LA) cells. Scale bars =100 µm.

Table 2. Apoptosis indices of free DOX, NPs, and DOX-loaded NCs. Data presented as mean ± standard deviation (SD) (n=3).

NPs/NCs/DOX	Apoptotic Index	
	HeLa Cells	**HEK293 Cells**
DOX	0.570 ± 0.030	0.021 ± 0.0040
SeAgChPEGFA NPs	0.056 ± 0.001	0.001 ± 0.0002
SeAgChPEGFA@DOX NCs	0.742 ± 0.051	0.002 ± 0.0001
F- SeAgChPEGFA NPs	0.062 ± 0.002	0.001 ± 0.0001
F- SeAgChPEGFA@DOX NCs	0.750 ± 0.034	0.003 ± 0.0002

V. Chapter Five: General Discussion, Conclusion, and Recommendations

Determining a safer and more efficient treatment for cancer has been an ongoing struggle since most of the existing treatments lack the competence to provide complete and specific eradication of this disease. Amongst the available treatments, chemotherapy remains one of the best ways to treat cancer because it attacks a vast array of cancer cells that cannot be removed through surgery or radiation. Despite its occasional successes, the treatment still requires improvement. The drugs used (administrated orally or intravenously) lack specificity making the treatment ineffective to provide long-lasting protection against cancer in addition to causing damage to healthy cells, organs, and tissues. This leads to severe side effects and the recurrence of the tumor after the discontinuation of the drug administration. Given the vitality of this treatment, resolving its limiting aspects by developing a system that shields the drugs from being used up by healthy cells, improving their specificity, and the way they are delivered will increase the chances of it working safer and more efficiently.

Currently, the merging of chemotherapy and nanotechnology to produce a platform called combination therapy seems to be a promising solution. Herein, metal nanoparticles derived from nanotechnology are used as therapeutics or anticancer drug-delivery systems due to their sophisticated properties. In this study selenium-silver bimetallic nanoparticles were chosen because of their enhanced catalytic properties and investigated as nanocarriers of doxorubicin. The carriers were formulated using two different synthesis methods, namely chemical and biological methods to evaluate the influence of each method on the effectiveness of the nano-systems as delivery vectors. The findings indicated that drug-loaded nanocomplexes produced using either of the two synthesis methods were able to effectively deliver doxorubicin to the cancer cells. In addition, the normal cells were insignificantly affected by these nanocomplexes, which indicates the specificity of the complexes. Therefore, this study indicates the potential of chitosan- polyethylene glycol stabilized folate targeted nanoparticles as effective delivery modalities for the anticancer drug, doxorubicin, in cancer cells *in vitro*.

Overall, it can be concluded that the use of stabilized nanoparticles to carry out receptor-mediated targeting of cancer cells is a promising approach to enhance chemotherapy. The synthesized novel selenium-silver nanoparticles have proven to be exceptional multifunctional (carrier and delivery) vectors owing to their attractive synergic properties and their ability to reduce the uptake of the drug by non-targeted cells and possible systemic toxicity. Moreover, the additional stabilization properties demonstrated by the biological method on the delivery system, emphasize the potential of the method to enhance characteristics needed for delivery systems which could facilitate applications in and out of the medical field.

Recommendations

The use of biosynthesized selenium and silver nanoparticles (individually) in cancer therapy (*in vitro* and *in vivo*) has been previously studied and reported to provide promising solutions to the challenges currently faced by traditional chemotherapy in efficient and safe drug delivery. However, the effects of these nanoparticles as a combined system had not yet been fully explored, thus, emphasizing the need to replicate this *in vitro* work in an *in vivo* system. This will help broadly evaluate the bimetallic system's safety and exact immune response and effect on major organs before using these NPs clinically. Following the *in vivo* evaluation of the bimetallic nanoparticles in cervical cancer, other cells with folate receptors should be subjected to treatment with these nanoparticles to ascertain the degree of their effectiveness in these cells as compared to their effectiveness in HeLa cells. The drug transported can also be changed to determine the system's flexibility andability to deliver alternative drugs other than doxorubicin. Lastly, future studies on thesenovel delivery systems should also focus on the delivery of various therapeutic genes to target cells, tissues, and organs, to further validate the multifunctionality of these bimetallic nanoparticles and eradicate any underlying chances of drug toxicity and resistance.

VI. Bibliography

Abdellatif, A.A., Mohammed, H.A., Khan, R.A., Singh, V., Bouazzaoui, A., Yusuf, M., Akhtar, N., Khan, M., Al-Subaiyel, A., Mohammed, S.A. and Al-Omar, M.S. 2021. Nano-scale delivery: a comprehensive review of nano-structured devices, preparative techniques, site-specificity designs, biomedical applications, commercial products, and references to safety, cellular uptake, and organ toxicity. *Nanotechnology Reviews*, 10, pp.1493-1559.

Agarwal, M., Agarwal, M. K., Shrivastav, N., Pandey, S., Das, R. and Gaur, P. 2018. Preparation of chitosan nanoparticles and their *in-vitro* characterization. *International Journal of Life-Sciences Scientific Research*, 4, pp.1713-1720.

Ahmad, N., Sharma, S., Singh, V.N., Shamsi, S.F., Fatma, A. and Mehta, B.R. 2011. Biosynthesis of silver nanoparticles from *Desmodium triflorum*: a novel approach towards weed utilization. *Biotechnology Research International*, 2011, pp. 1-8.

Ahmad, A., Alghamdi, S. S., Mahmood, K. and Afzal, M. 2016. Fenugreek a multipurpose crop: potentialities and improvements. *Saudi Journal of Biological Sciences*, 23, pp.300-310.

Aibani, N., Rai, R., Patel, P., Cuddihy, G. and Wasan, E.K. 2021. Chitosan nanoparticles at the biological interface: implications for drug delivery. *Pharmaceutics*, 13, p.1686.

Akinyelu, J. and Singh, M. 2019. Folate-tagged chitosan-functionalized gold nanoparticles for enhanced delivery of 5-fluorouracil to cancer cells. *Applied Nanoscience*, 9, pp.7-17.

Al Rifai, R. and Nakamura, K. 2015. Differences in breast and cervical cancer screening rates in Jordan among women from different socioeconomic strata: analysis of the 2012 population-based household survey. *Asian Pacific Journal of Cancer Prevention*, 16, pp.6697-6704.

Alagesan, V. and Venugopal, S. 2019. Green synthesis of selenium nanoparticle using leaves extract of *Withania somnifera* and its biological applications and photocatalytic activities. *Bionanoscience*, 9, pp.105-116.

Alam, H., Khatoon, N., Raza, M., Ghosh, P. C. and Sardar, M. 2019. Synthesis and characterization of nano selenium using plant biomolecules and their potential applications. *Bionanoscience*, 9, pp.96-104.

Almatroodi, S.A., Almatroudi, A., Alsahli, M.A. and Rahmani, A.H. 2021. Fenugreek (*Trigonella foenum-graecum*) and its active compounds: a review of its effects on human health through modulating biological activities. *Pharmacognosy Journal*, 13, pp.813-821.

Alshatwi, A.A., Athinarayanan, J. and Periasamy, V.S. 2015. Green synthesis of bimetallic Au@ Pt nanostructures and their application for proliferation inhibition and apoptosis induction in human cervical cancer cell. *Journal of Materials Science*: *Materials in Medicine*, 26, pp.1-9.

Alwhibi, M. S., Soliman, D. A., Awad, M. A., Rizwana, H. and Marraiki, N. A. 2018. Biosynthesis of silver nanoparticles using fenugreek seed extract and evaluation of their antifungal and antibacterial activities. *Journal of Computational and Theoretical Nanoscience*, 15, pp.1255-1260.

Amany, A., El-Rab, S.F.G. and Gad, F. 2012. Effect of reducing and protecting agents on size of silver nanoparticles and their anti-bacterial activity. *Der Pharma Chemica*, 4, pp.53-65.

Angelopoulou, A., Kolokithas-Ntoukas, A., Fytas, C. and Avgoustakis, K. 2019. Folic acid-functionalized, condensed magnetic nanoparticles for targeted delivery of doxorubicin to tumor cancer cells overexpressing the folate receptor. *ACS Omega*, 4, pp.22214-22227.

Anitha, M. L., Riya, J., Rinita, J., Eunice, P. C. and Jothi, N. N. 2021. Facile green synthesis and characterisation of gold nanoparticles using fenugreek seeds and honey. *Journal of Physics: Conference Series*, 2070, p.012048.

Annamalai, A., Christina, V.L.P., Sudha, D., Kalpana, M. and Lakshmi, P.T.V. 2013. Green synthesis, characterization and antimicrobial activity of Au NPs using *Euphorbia hirta L*. leaf extract. *Colloids and Surfaces B: Biointerfaces*, 108, pp.60-65.

Atta, N.F., Gawad, S.A.A., Galal, A., Razik, A.A. and El-Gohary, A.R. 2021. Efficient electrochemical sensor for determination of H_2O_2 in human serum based on nano iron-nickel alloy/carbon nanotubes/ionic liquid crystal composite. *Journal of Electroanalytical Chemistry*, 881, p.114953.

Azadpour, A., Hajrasouliha, S. and Khaleghi, S. 2022. Green synthesized-silver nanoparticles coated with targeted chitosan nanoparticles for smart drug delivery. *Journal of Drug Delivery Science and Technology*, 74, p.103554.

Baskar, R., Lee, K.A., Yeo, R. and Yeoh, K.W. 2012. Cancer and radiation therapy: current advances and future directions. *International Journal of Medical Sciences*, 9, p.193.

Bauer, A.T., Strozyk, E.A., Gorzelanny, C., Westerhausen, C., Desch, A., Schneider, M.F. and Schneider, S.W. 2011. Cytotoxicity of silica nanoparticles through exocytosis of von Willebrand factor and necrotic cell death in primary human endothelial cells. *Biomaterials*, 32, pp.8385-8393.

Bazak, R., Houri, M., El Achy, S., Kamel, S. and Refaat, T. 2015. Cancer active targeting by nanoparticles: a comprehensive review of literature. *Journal of Cancer Research and Clinical Oncology*, 141, pp.769-784.

Berrouet, C., Dorilas, N., Rejniak, K.A. and Tuncer, N., 2020. Comparison of drug inhibitory effects (IC_{so}) in monolayer and spheroid cultures. *Bulletin of Mathematical Biology*, 82, p.68

Beyene, H.D., Werkneh, A.A., Bezabh, H.K. and Ambaye, T.G., 2017. Synthesis paradigm and applications of silver nanoparticles (AgNPs): a review. *Sustainable Materials and Technologies,* 13, pp.18-23.

Brady, B., Wang, P. H., Steenhoff, V. and Brolo, A. G. 2019. Nanostructuring solar cells using metallic nanoparticles. *Metal Nanostructures for Photonics*, 2019, pp.197-221.

Burdușel, A.-C., Gherasim, O., Grumezescu, A. M., Mogoantă, L., Ficai, A. and Andronescu, E. 2018. Biomedical applications of silver nanoparticles: an up-to-date overview. *Nanomaterials*, 8, p.681.

Carlson, L. E., Waller, A. and Mitchell, A. J. 2012. Screening for distress and unmet needs in patients with cancer: review and recommendations. *Journal of Clinical Oncology*, 30, pp.1160-1177.

Chalati, T., Horcajada, P., Gref, R., Couvreur, P. and Serre, C. 2011. Optimisation of the synthesis of MOF nanoparticles made of flexible porous iron fumarate MIL-88A. *Journal of Materials Chemistry*, 21, pp.2220-2227.

Chen, X., Zou, L.-Q., Niu, J., Liu, W., Peng, S.-F. and Liu, C.-M. 2015. The stability, sustained release and cellular antioxidant activity of curcumin nanoliposomes. *Molecules*, 20, pp.14293-14311.

Chu, E. and Sartorelli, A.C. 2018. Cancer chemotherapy. *Lange's Basic and Clinical Pharmacology*, 2018, pp.948-976.

Clogston, J. D. and Patri, A. 2011. Zeta Potential Measurement. In: McNeil, S. (eds) characterization of nanoparticles intended for drug delivery. *Methods in Molecular Biology*, 697, p.697.

Colson, P., Henrist, C. and Cloots, R. 2013. Nanosphere lithography: a powerful method for the controlled manufacturing of nanomaterials. *Journal of Nanomaterials*, 2013, p.21.

Collado-González, M., Montalbán, M.G., Peña-García, J., Pérez-Sánchez, H., Víllora, G. and Baños, F.G.D. 2017. Chitosan as stabilizing agent for negatively charged nanoparticles. *Carbohydrate Polymers*, 161, pp.63-70.

Cordani, M. and Somoza, Á. 2019. Targeting autophagy using metallic nanoparticles: a promising strategy for cancer treatment. *Cellular and Molecular Life Sciences*, 76, pp.1215-1242.

Dang, Y. and Guan, J. 2020. Nanoparticle-based drug delivery systems for cancer therapy. *Smart Materials in Medicine*, 1, pp.10-19.

Davenport, S.M., Suidan, R.S., Huang, J., Hyman, D.M. and Chi, D.S. 2015. Primary debulking surgery for metastatic cervical adenocarcinoma: a case report. *Gynecologic Oncology Reports*, 14, p.23.

Daniels, A. N. and Singh, M. 2019. Sterically stabilized siRNA: gold nanocomplexes enhance c-MYC silencing in a breast cancer cell model. *Nanomedicine*, 14, pp.1387-1401.

de Barros, A.B., Tsourkas, A., Saboury, B., Cardoso, V.N. and Alavi, A. 2012. Emerging role of radiolabeled nanoparticles as an effective diagnostic technique. *EJNMMI Research*, 2, pp.1-15.

De Trizio, A., Srisuk, P., Costa, R. R., Fraga, A. G., Modena, T., Genta, I., Dorati, R., Pedrosa, J., Conti, B. and Correlo, V. M. 2017. Natural based eumelanin nanoparticles functionalization and preliminary evaluation as carrier for gentamicin. *Reactive and Functional Polymers*, 114, pp.38-48.

Deshmukh, A.R., Gupta, A. and Kim, B.S. 2019. Ultrasound assisted green synthesis of silver and iron oxide nanoparticles using fenugreek seed extract and their enhanced antibacterial and antioxidant activities. *BioMed Research International*, 2019, pp.1-14.

Dhall, A. and Self, W. 2018. Cerium oxide nanoparticles: a brief review of their synthesis methods and biomedical applications. *Antioxidants*, 7, p.97.

Du, J.-Z., Mao, C.-Q., Yuan, Y.-Y., Yang, X.-Z. and Wang, J. 2014. Tumor extracellular acidity-activated nanoparticles as drug delivery systems for enhanced cancer therapy. *Biotechnology Advances*, 32, pp.789-803.

Duan, M., Jiang, L., Zeng, G., Wang, D., Tang, W., Liang, J., Wang, H., He, D., Liu, Z. and Tang, L. 2020. Bimetallic nanoparticles/metal-organic frameworks: synthesis, applications and challenges. *Applied Materials Today*, 19, p.100564.

Elemike, E.E., Onwudiwe, D.C., Fayemi, O.E. and Botha, T.L. 2019. Green synthesis and electrochemistry of Ag, Au, and Ag–Au bimetallic nanoparticles using golden rod (*Solidago canadensis*) leaf extract. *Applied Physics A*, 125, pp.1-12.

El-Seedi, H. R., El-Shabasy, R. M., Khalifa, S. A., Saeed, A., Shah, A., Shah, R., Iftikhar, F. J., Abdel-Daim, M. M., Omri, A. and Hajrahand, N. H. 2019. Metal nanoparticles fabricated by green chemistry using natural extracts: biosynthesis, mechanisms, and applications. *RSC Advances*, 9, pp.24539-24559.

Fardsadegh, B. and Jafarizadeh-Malmiri, H. 2019. Aloe vera leaf extract mediated green synthesis of selenium nanoparticles and assessment of their *in vitro* antimicrobial activity against spoilage fungi and pathogenic bacteria strains. *Green Processing and Synthesis*, 8, pp.399-407.

Fazio, E., Gökce, B., De Giacomo, A., Meneghetti, M., Compagnini, G., Tommasini, M., Waag, F., Lucotti, A., Zanchi, C. G. and Ossi, P. M. 2020. Nanoparticles engineering by pulsed laser ablation in liquids: concepts and applications. *Nanomaterials*, 10, p.2317.

Fernández-Villa, D., Jiménez Gómez-Lavín, M., Abradelo, C., San Román, J. and Rojo, L., 2018. Tissue engineering therapies based on folic acid and other vitamin B derivatives. functional mechanisms and current applications in regenerative medicine. *International Journal of Molecular Sciences*, 19, p.4068.

Förster, H., Wolfrum, C. and Peukert, W. 2012. Experimental study of metal nanoparticle synthesis by an arc evaporation/condensation process. *Journal of Nanoparticle Research*, 14, pp.1-16.

Frank, L., Onzi, G., Morawski, A., Pohlmann, A., Guterres, S. and Contri, R. 2020. Chitosan as a coating material for nanoparticles intended for biomedical applications. *Reactive and Functional Polymers*, 147, p.104459.

Frigaard, J., Jensen, J.L., Galtung, H.K. and Hiorth, M., 2022. The potential of chitosan in nanomedicine: an overview of the cytotoxicity of chitosan based nanoparticles. *Frontiers in Pharmacology*, 13, p.1492.

Ghosh, N. and Singh, R. 2021. *In vitro* cytotoxicity assay of biogenically synthesized bimetallic nanoparticles. *Rasayan J. Chem*, 14, pp.486-492.

Gillich, T., Acikgöz, C., Isa, L., Schlüter, A.D., Spencer, N.D. and Textor, M. 2013. PEG-stabilized core–shell nanoparticles: impact of linear versus dendritic polymer shell architecture on colloidal properties and the reversibility of temperature-induced aggregation. *American Chemical Society Nano*, 7, pp.316-329.

Grzelczak, M., Sánchez-Iglesias, A., Rodríguez-González, B., Alvarez-Puebla, R., Pérez-Juste, J. and Liz-Marzán, L.M. 2008. Influence of iodide ions on the growth of gold nanorods: tuning tip curvature and surface plasmon resonance. *Advanced Functional Materials*, 18, pp.3780-3786.

Gulati, S., Sachdeva, M. and Bhasin, K.K. 2018. Capping agents in nanoparticle synthesis: surfactant and solvent system. *AIP Conference Proceedings,* 1953, p.030214.

Gurram, L., Kalra, B. and Mahantshetty, U. 2020. Meeting the global need for radiation therapy in cervical cancer: an overview. *Seminars in Radiation Oncology,* 30, pp. 348-354.

Güzel, R. and Erdal, G. 2018 Synthesis of silver nanoparticles. In *Silver Nanoparticles: Fabrication, Characterization and Applications,* Maaz, K., Ed.; IntechOpen: London, UK, pp. 1-20.

Harris, N., Blaber, M.G. and Schatz, G.C. 2012. Optical properties of metal nanoparticles. *Encyclopedia of Nanotechnology*, 481, pp.9751-9754.

Hefni, H.H., Azzam, E.M., Badr, E.A., Hussein, M. and Tawfik, S.M. 2016. Synthesis, characterization and anticorrosion potentials of chitosan-g-PEG assembled on silver nanoparticles. *International Journal of Biological Macromolecules*, 83, pp.297-305.

Hembram, K. C., Kumar, R., Kandha, L., Parhi, P. K., Kundu, C. N. and Bindhani, B. K. 2018. Therapeutic prospective of plant-induced silver nanoparticles: application as

antimicrobial and anticancer agent. *Artificial Cells, Nanomedicine, and Biotechnology*, 46, pp.38-51.

Hosseini Bafghi, M., Safdari, H., Nazari, R., Darroudi, M., Sabouri, Z., Zargar, M. and Zarrinfar, H. 2021. Evaluation and comparison of the effects of biosynthesized selenium and silver nanoparticles using plant extracts with antifungal drugs on the growth of *Aspergillus* and *Candida* species. *Rendiconti Lincei. Scienze Fisiche e Naturali*, 32, pp.791-803.

Huang, H. and Yang, X. 2004. Synthesis of chitosan-stabilized gold nanoparticles in the absence/presence of tripolyphosphate. *Biomacromolecules*, 5, pp.2340-2346.

Huy, T. Q., Huyen, P., Le, A.-T. and Tonezzer, M. 2020. Recent advances of silver nanoparticles in cancer diagnosis and treatment. *Anti-Cancer Agents in Medicinal Chemistry (Formerly Current Medicinal Chemistry-Anti-Cancer Agents)*, 20, pp.1276-1287.

Ijaz, M., Zafar, M. and Iqbal, T. 2020. Green synthesis of silver nanoparticles by using various extracts: a review. *Inorganic and Nano-Metal Chemistry*, 51, pp.744-755.

Ikram, M., Javed, B. and Raja, N.I. 2021. Biomedical potential of plant-based selenium nanoparticles: a comprehensive review on therapeutic and mechanistic aspects. *International Journal of Nanomedicine*, 16, p.249.

Iqbal, D., Hassan, A., Ansari, A. A., Muhammad, N., Khan, A., Khalid, S. and Sharif, F. 2022. Sustainable silver nanoparticles as the vector for green therapeutics in oncology. *Applied Nanoscience*, 12, pp.1425-1434.

Ishak, N. M., Kamarudin, S. and Timmiati, S. 2019. Green synthesis of metal and metal oxide nanoparticles via plant extracts: an overview. *Materials Research Express*, 6, p.112004.

Iravani, S., Korbekandi, H., Mirmohammadi, S.V. and Zolfaghari, B. 2014. Synthesis of silver nanoparticles: chemical, physical and biological methods. *Research in Pharmaceutical Sciences*, 9, p.385.

Ivanova, N., Gugleva, V., Dobreva, M., Pehlivanov, I., Stefanov, S. and Andonova, V. 2018. Silver nanoparticles as multi-functional drug delivery systems. In *Nanomedicines,* IntechOpen, pp.71-91.

Jabłońska, E. and Reszka, E. 2017. Selenium and epigenetics in cancer: focus on DNA methylation. *Advances in Cancer Research*, 136, pp.193-234.

Jadoun, S., Arif, R., Jangid, N. K. and Meena, R. K. 2021. Green synthesis of nanoparticles using plant extracts: a review. *Environmental Chemistry Letters*, 19, pp.355-374.

Jamkhande, P. G., Ghule, N. W., Bamer, A. H. and Kalaskar, M. G. 2019. Metal nanoparticles synthesis: an overview on methods of preparation, advantages and disadvantages, and applications. *Journal of Drug Delivery Science and Technology*, 53, p.101174.

Jana, J., Ganguly, M. and Pal, T. 2016. Enlightening surface plasmon resonance effect of metal nanoparticles for practical spectroscopic application. *RSC Advances*, 6, pp.86174-86211.

Judefeind, A. and de Villiers, M.M. 2009. Drug loading into and *in vitro* release from nanosized drug delivery systems. *Nanotechnology in Drug Delivery*, 10, pp.129-162.

Khandel, P., Yadaw, R.K., Soni, D.K., Kanwar, L. and Shahi, S.K. 2018. Biogenesis of metal nanoparticles and their pharmacological applications: present status and application prospects. *Journal of Nanostructure in Chemistry*, 8, pp.217-254.

Khurana, A., Tekula, S., Saifi, M. A., Venkatesh, P. and Godugu, C. 2019. Therapeutic applications of selenium nanoparticles. *Biomedicine and Pharmacotherapy*, 111, pp.802-812.

Kiranmai, M. 2017. Biological and non-biological synthesis of metallic nanoparticles: scope for current pharmaceutical research. *Indian Journal of Pharmaceutical Sciences*, 79, pp.501-512.

Kor, N. and Moradi, K. 2013. Effect of fenugreek (*Trigonella foenum-graecum*) on production indices in Loman lsl-lite hens. *Online Journal of Veterinary Research*, 17, pp.323-328.

Krishnaraj, C., Radhakrishnan, S., Ramachandran, R., Ramesh, T., Kim, B.-S. and Yun, S.-I. 2022. *In vitro* toxicological assessment and biosensing potential of bioinspired chitosan nanoparticles, selenium nanoparticles, chitosan/selenium nanocomposites, silver nanoparticles and chitosan/silver nanocomposites. *Chemosphere*, 301, p.134790.

Kulkarni, S.A. and Feng, S.S. 2013. Effects of particle size and surface modification on cellular uptake and biodistribution of polymeric nanoparticles for drug delivery. *Pharmaceutical Research*, 30, pp.2512-2522.

Leamon, C. P., Vlahov, I. R., Reddy, J. A., Vetzel, M., Santhapuram, H. K. R., You, F., Bloomfield, A., Dorton, R., Nelson, M. and Kleindl, P. 2014. Folate–vinca alkaloid conjugates for cancer therapy: a structure–activity relationship. *Bioconjugate Chemistry*, 25, pp.560-568.

Lee, J.W., Choi, S.R. and Heo, J.H. 2021. Simultaneous stabilization and functionalization of gold nanoparticles via biomolecule conjugation: progress and perspectives. *ACS Applied Materials and Interfaces*, 13, pp.42311-42328.

Liang, J., Zhang, Z., Zhao, H., Wan, S., Zhai, X., Zhou, J., Liang, R., Deng, Q., Wu, Y. and Lin, G. 2018. Simple and rapid monitoring of doxorubicin using streptavidin-modified microparticle-based time-resolved fluorescence immunoassay. *RSC Advances*, 8, pp.15621-15631.

Ligasová, A. and Koberna, K. 2021. DNA dyes—highly sensitive reporters of cell quantification: comparison with other cell quantification methods. *Molecules*, 26, p.5515.

Liu, E.T. 2003. Classification of cancers by expression profiling. *Current Opinion in Genetics and Development*, 13, pp.97-103.

Liu, K., Liu, P.C., Liu, R. and Wu, X. 2015. Dual AO/EB staining to detect apoptosis in osteosarcoma cells compared with flow cytometry. *Medical Science Monitor Basic Research*, 21, p.15.

Liu, F., Liu, H., Liu, R., Xiao, C., Duan, X., McClements, D.J. and Liu, X., 2019. Delivery of sesamol using polyethylene-glycol-functionalized selenium nanoparticles in human liver cells in culture. *Journal of Agricultural and Food Chemistry*, 67, pp.2991-2998.

Liu, Q., Zhao, X., Ma, J., Mu, Y., Wang, Y., Yang, S., Wu, Y., Wu, F. and Zhou, Y. 2021. Selenium (Se) plays a key role in the biological effects of some viruses: implications for COVID-19. *Environmental Research*, 196, p.110984.

Luesakul, U., Puthong, S., Neamati, N. and Muangsin, N. 2018. pH-responsive selenium nanoparticles stabilized by folate-chitosan delivering doxorubicin for overcoming drug-resistant cancer cells. *Carbohydrate Polymers*, 181, pp.841-850.

Maiyo, F. and Singh, M. 2017. Selenium nanoparticles: potential in cancer gene and drug delivery. *Nanomedicine*, 12, pp.1075-1089.

Maiyo, F. and Singh, M. 2019. Folate-targeted mRNA delivery using chitosan-functionalized selenium nanoparticles: potential in cancer immunotherapy. *Pharmaceuticals*, 12, p.164.

Maiyo, F. and Singh, M. 2020. Polymerized selenium nanoparticles for folate-receptor-targeted delivery of anti-Luc-siRNA: potential for gene silencing. *Biomedicines*, 8, p.76.

Malinga, T., Kudanga, T. and Mbatha, L.S., 2021. Stealth doxorubicin conjugated bimetallic selenium/silver nanoparticles for targeted cervical cancer therapy. *Advances in Natural Sciences: Nanoscience and Nanotechnology*, 12, p.045006.

Maney, V. and Singh, M. 2017. An *in vitro* assessment of novel chitosan/bimetallic PtAu nanocomposites as delivery vehicles for doxorubicin. *Nanomedicine*, 12, pp.2625-2640.

Maney, V. and Singh, M. 2019. The synergism of platinum-gold bimetallic nanoconjugates enhances 5-fluorouracil delivery *in vitro*. *Pharmaceutics*, 11, p.439.

Manke, A., Wang, L. and Rojanasakul, Y. 2013. Mechanisms of nanoparticle-induced oxidative stress and toxicity. *BioMed Research International*, 2013, pp.1-15.

Mavani, K. and Shah, M. 2013. Synthesis of silver nanoparticles by using sodium borohydride as a reducing agent. *International Journal of Engineering Research and Technology*, 2, pp.1-5.

Mbatha, L. S. and Singh, M. 2019. Starburst poly (amidoamine) dendrimer grafted gold nanoparticles as a scaffold for folic acid-targeted plasmid DNA delivery *in vitro*. *Journal of Nanoscience and Nanotechnology*, 19, pp.1959-1970.

Menon, S., Ks, S. D., Santhiya, R., Rajeshkumar, S. and Kumar, V. 2018. Selenium nanoparticles: a potent chemotherapeutic agent and an elucidation of its mechanism. *Colloids and Surfaces B: Biointerfaces*, 170, pp.280-292.

Mikhailov, O. V. and Mikhailova, E. O. 2019. Elemental silver nanoparticles: biosynthesis and bio applications. *Materials*, 12, p.3177.

Miranda, R. R., Sampaio, I. and Zucolotto, V. 2022. Exploring silver nanoparticles for cancer therapy and diagnosis. *Colloids and Surfaces B: Biointerfaces*, 210, p.112254.

Modan, E. M. and Plăiașu, A. G. 2020. Advantages and disadvantages of chemical methods in the elaboration of nanomaterials. *The Annals of "Dunarea de Jos" University of Galati. Fascicle IX, Metallurgy and Materials Science*, 43, pp.53-60.

Mohammadinejad, R., Moosavi, M.A., Tavakol, S., Vardar, D.Ö., Hosseini, A., Rahmati, M., Dini, L., Hussain, S., Mandegary, A. and Klionsky, D.J. 2019. Necrotic, apoptotic and autophagic cell fates triggered by nanoparticles. *Autophagy*, 15, pp.4-33.

Naikoo, G. A., Mustaqeem, M., Hassan, I. U., Awan, T., Arshad, F., Salim, H. and Qurashi, A. 2021. Bioinspired and green synthesis of nanoparticles from plant extracts with antiviral and antimicrobial properties: a critical review. *Journal of Saudi Chemical Society*, 25, pp.101304.

Nayak, D., Ashe, S., Rauta, P. R., Kumari, M. and Nayak, B. 2016. Bark extract mediated green synthesis of silver nanoparticles: evaluation of antimicrobial activity and antiproliferative response against osteosarcoma. *Materials Science and Engineering: C*, 58, pp.44-52.

Nikoletopoulou, V., Markaki, M., Palikaras, K. and Tavernarakis, N. 2013. Crosstalk between apoptosis, necrosis and autophagy. *Biochimica et Biophysica Acta (BBA)-Molecular Cell Research*, 1833, pp.3448-3459.

Okugawa, K., Yahata, H., Sonoda, K., Kodama, K., Yagi, H., Ohgami, T., Yasunaga, M., Onoyama, I., Kaneki, E. and Asanoma, K. 2021. Evaluation of adjuvant chemotherapy after abdominal trachelectomy for cervical cancer: a single-institution experience.*International Journal of Clinical Oncology*, 26, pp.216-224.

Oladipo, A.O., Iku, S.I., Ntwasa, M., Nkambule, T.T., Mamba, B.B. and Msagati, T.A. 2020. Doxorubicin conjugated hydrophilic AuPt bimetallic nanoparticles fabricated from *Phragmites australis*: characterization and cytotoxic activity against human cancer cells. *Journal of Drug Delivery Science and Technology*, 57, p.101749.

Olawale, F., Ariatti, M. and Singh, M. 2021. Biogenic synthesis of silver-core selenium-shell nanoparticles using *Ocimum tenuiflorum L.*: response surface methodology-based optimization and biological activity. *Nanomaterials*, 11, p.2516.

Panzarini, E., Mariano, S. and Dini, L. 2015. Glycans coated silver nanoparticles induces autophagy and necrosis in HeLa cells. *AIP Conference Proceedings*, 1667, p.020017.

Parhi, R., 2020. Drug delivery applications of chitin and chitosan: a review. *Environmental Chemistry Letters*, 18, pp.577-594.

Park, S. Y., Lee, C. Y., An, H.-R., Kim, H., Lee, Y.-C., Park, E. C., Chun, H.-S., Yang, H. Y., Choi, S.-H. and Kim, H. S. 2017. Advanced carbon dots via plasma-induced surface functionalization for fluorescent and bio-medical applications. *Nanoscale*, 9, pp.9210-9217.

Paszkiewicz, M., Gołąbiewska, A., Rajski, Ł., Kowal, E., Sajdak, A. and Zaleska-Medynska, A. 2016. Synthesis and characterization of monometallic (Ag, Cu) and bimetallic Ag-Cu particles for antibacterial and antifungal applications. *Journal of Nanomaterials*, 2016, p.6.

Patel, A. 2020. Benign vs malignant tumors. *JAMA Oncology*, 6, pp.1488-1488.

Patra, D.K., Pradhan, C. and Patra, H.K., 2018. Chelate based phytoremediation study for attenuation of chromium toxicity stress using lemongrass: *Cymbopogon flexuosus* (nees ex steud.) W. Watson. *International Journal of Phytoremediation*, 20, pp.1324-1329.

Peter, S., Alven, S., Maseko, R.B. and Aderibigbe, B.A. 2022. Doxorubicin-based hybrid compounds as potential anticancer agents: a review. *Molecules*, 27, p.4478.

Pi, J., Jin, H., Liu, R., Song, B., Wu, Q., Liu, L., Jiang, J., Yang, F., Cai, H. and Cai, J. 2013. Pathway of cytotoxicity induced by folic acid modified selenium nanoparticles in MCF-7 cells. *Applied Microbiology and Biotechnology*, 97, pp.1051-1062.

Pyrzynska, K. and Sentkowska, A. 2021. Biosynthesis of selenium nanoparticles using plant extracts. *Journal of Nanostructure in Chemistry*, 12, pp.467-480.

Rafiei, P. and Haddadi, A. 2017. Docetaxel-loaded PLGA and PLGA-PEG nanoparticles for intravenous application: pharmacokinetics and biodistribution profile. *International Journal of Nanomedicine*, 12, p.935.

Rahimi, H.R. and Doostmohammadi, M. 2019. Nanoparticle synthesis, applications, and toxicity. *Applications of Nanobiotechnology*, IntechOpen, 2019, pp.1-16.

Ramamurthy, C.H., Sampath, K.S., Arunkumar, P., Kumar, M.S., Sujatha, V., Premkumar, K. and Thirunavukkarasu, C. 2013. Green synthesis and characterization of selenium nanoparticles and its augmented cytotoxicity with doxorubicin on cancer cells. *Bioprocess and Biosystems Engineering*, 36, pp.1131-1139.

Ramirez, P.T., Pareja, R., Rendón, G.J., Millan, C., Frumovitz, M. and Schmeler, K.M. 2014. Management of low-risk early-stage cervical cancer: should conization, simple trachelectomy, or simple hysterectomy replace radical surgery as the new standard of care?. *Gynecologic Oncology*, 132, pp.254-259.

Rennick, J.J., Johnston, A.P. and Parton, R.G. 2021. Key principles and methods for studying the endocytosis of biological and nanoparticle therapeutics. *Nature Nanotechnology*, 16, pp.266-276.

Richard, I., Thibault, M., De Crescenzo, G., Buschmann, M.D. and Lavertu, M. 2013. Ionization behavior of chitosan and chitosan–DNA polyplexes indicate that chitosan has a similar capability to induce a proton-sponge effect as PEI. *Biomacromolecules*, 14, pp.1732-1740.

Ridolfo, R., Tavakoli, S., Junnuthula, V., Williams, D.S., Urtti, A. and van Hest, J.C. 2020. Exploring the impact of morphology on the properties of biodegradable nanoparticles and their diffusion in complex biological medium. *Biomacromolecules,* 22, pp.126-133.

Rizvi, S. A. and Saleh, A. M. 2018. Applications of nanoparticle systems in drug delivery technology. *Saudi Pharmaceutical Journal*, 26, pp.64-70.

Ruiz-Fresneda, M. A., Eswayah, A. S., Romero-González, M., Gardiner, P. H., Solari, P. L. and Merroun, M. L. 2020. Chemical and structural characterization of Se IV biotransformations by *Stenotrophomonas bentonitica* into Se 0 nanostructures and volatiles Se species. *Environmental Science: Nano*, 7, pp.2140-2155.

Saini, A., Kumar, M., Bhatt, S., Saini, V. and Malik, A. 2020. Cancer causes and treatments. *International Journal of Pharmaceutical Sciences and Research*, 11, pp.3121-3134.

Saraste, A. and Pulkki, K. 2000. Morphologic and biochemical hallmarks of apoptosis. *Cardiovascular Research,* 45, pp.528-537.

Saravanan, A., Kumar, P. S., Karishma, S., Vo, D.-V. N., Jeevanantham, S., Yaashikaa, P. and George, C. S. 2021. A review on biosynthesis of metal nanoparticles and its environmental applications. *Chemosphere*, 264, p.128580.

Scaranti, M., Cojocaru, E., Banerjee, S. and Banerji, U. 2020. Exploiting the folate receptor α in oncology. *Nature Reviews Clinical Oncology*, 17, pp.349-359.

Senapati, S., Mahanta, A. K., Kumar, S. and Maiti, P. 2018. Controlled drug delivery vehicles for cancer treatment and their performance. *Signal Transduction and Targeted Therapy*, 3, pp.1-19.

Shariatinia, Z. 2019. Pharmaceutical applications of chitosan. *Advances in Colloid and Interface Science*, 263, pp.131-194.

Sharma, P., Mehta, M., Dhanjal, D. S., Kaur, S., Gupta, G., Singh, H., Thangavelu, L., Rajeshkumar, S., Tambuwala, M. and Bakshi, H. A. 2019. Emerging trends in the novel drug delivery approaches for the treatment of lung cancer. *Chemico-Biological Interactions*, 309, p.108720.

Shkhair, A.I., Jabber, M.K., A-Kadhim, M.H. and Jabber, A.H. 2018. Chemical synthesis and characterization of silver nanoparticles induced biocompatibility for anticancer activity. *Executive Editor*, 9, p.352.

Singh, M. and Ariatti, M. 2003. Targeted gene delivery into HepG2 cells using complexes containing DNA, cationized asialoorosomucoid and activated cationic liposomes. *Journal of Controlled Release*, 92, pp.383-394.

Sithole, N.T., Ntuli, F. and Mashifana, T. 2018. The removal of Cu (II) from aqueous solution using sodium borohydride as a reducing agent. *IOP Conference Series: Earth and Environmental Science,* 120, p.012022.

Siwowska, K., Schmid, R.M., Cohrs, S., Schibli, R. and Müller, C., 2017. Folate receptor-positive gynecological cancer cells: *in vitro* and *in vivo* characterization. *Pharmaceuticals*, 10, p.72.

Small Jr, W., Bacon, M. A., Bajaj, A., Chuang, L. T., Fisher, B. J., Harkenrider, M. M., Jhingran, A., Kitchener, H. C., Mileshkin, L. R. and Viswanathan, A. N. 2017. Cervical cancer: a global health crisis. *Cancer*, 123, pp.2404-2412.

Sohn, S., Xie, Y., Jung, Y., Schroers, J. and Cha, J. J. 2017. Tailoring crystallization phases in metallic glass nanorods via nucleus starvation. *Nature Communications*, 8, pp.1-8.

Sorbiun, M., Shayegan Mehr, E., Ramazani, A. and Mashhadi Malekzadeh, A. 2018. Biosynthesis of metallic nanoparticles using plant extracts and evaluation of their antibacterial properties. *Nanochemistry Research*, 3, pp.1-16.

Sportelli, M. C., Izzi, M., Volpe, A., Clemente, M., Picca, R. A., Ancona, A., Lugarà, P. M., Palazzo, G. and Cioffi, N. 2018. The pros and cons of the use of laser ablation synthesis for the production of silver nano-antimicrobials. *Antibiotics*, 7, p.67.

Srivastava, P. and Kowshik, M. 2016. Anti-neoplastic selenium nanoparticles from *Idiomarina sp*. PR58-8. *Enzyme and Microbial Technology*, 95, pp.192-200.

Sung, H., Ferlay, J., Siegel, R. L., Laversanne, M., Soerjomataram, I., Jemal, A. and Bray, F. 2021. Global cancer statistics 2020: GLOBOCAN estimates of incidence and mortality worldwide for 36 cancers in 185 countries. *CA: a cancer journal for clinicians,* 71(3), pp.209-249.

Tannock, I.F. 1989. Combined modality treatment with radiotherapy and chemotherapy. *Radiotherapy and Oncology*, 16, pp.83-101.

Tempfer, C. B., Tischoff, I., Dogan, A., Hilal, Z., Schultheis, B., Kern, P. and Rezniczek, G. A. 2018. Neuroendocrine carcinoma of the cervix: a systematic review of the literature. *BMC Cancer*, 18, pp.1-16.

Thariat, J., Hannoun-Levi, J.M., Sun Myint, A., Vuong, T. and Gérard, J.P. 2013. Past, present, and future of radiotherapy for the benefit of patients. *Nature Reviews Clinical Oncology*, 10, pp.52-60.

Truong, N.P., Whittaker, M.R., Mak, C.W. and Davis, T.P. 2015. The importance of nanoparticle shape in cancer drug delivery. *Expert Opinion on Drug Delivery*, 12, pp.129-142.

ul Hussain, H., Burney, M. H., Rehan, S. T. and Hasan, M. M. 2022. Dostarlimab: a

breakthrough in the field of oncology. *Annals of Medicine and Surgery*, 80, p.104046.

Vahdati, M. and Tohidi Moghadam, T. 2020. Synthesis and characterization of selenium nanoparticles-lysozyme nanohybrid system with synergistic antibacterial properties. *Scientific Reports,* 10, p.510.

Vaid, P., Raizada, P., Saini, A.K. and Saini, R.V. 2020. Biogenic silver, gold and copper nanoparticles: a sustainable green chemistry approach for cancer therapy. S*ustainable Chemistry and Pharmacy*, 16, p.100247.

Vergallo, C., Panzarini, E., Carata, E., Ahmadi, M., Mariano, S., Tenuzzo, B.A. and Dini, L. 2016. Cytotoxicity of β-D-glucose/sucrose-coated silver nanoparticles depends on cell type, nanoparticles concentration and time of incubation. *AIP Conference Proceedings,* 1749, p.020012.

Vodop'yanov, A., Mansfeld, D., Samokhin, A., Alekseev, N. and Tsvetkov, Y. V. 2017. Production of nanopowders by the evaporation–condensation method using a focused microwave radiation. *Radiophysics and Quantum Electronics*, 59, pp.698-705.

Wang, C., Yin, H., Chan, R., Peng, S., Dai, S. and Sun, S. 2009. One-pot synthesis of oleylamine coated AuAg alloy NPs and their catalysis for CO oxidation. *Chemistry of Materials*, 21, pp.433-435.

Wang, K., Zhuang, J., Liu, Y., Xu, M., Zhuang, J., Chen, Z., Wei, Y. and Zhang, Y. 2018. PEGylated chitosan nanoparticles with embedded bismuth sulfide for dual-wavelength fluorescent imaging and photothermal therapy. *Carbohydrate Polymers*, 184, pp.445-452.

Weitman, S.D., Lark, R.H., Coney, L.R., Fort, D.W., Frasca, V., Zurawski Jr, V.R. and Kamen, B.A. 1992. Distribution of the folate receptor GP38 in normal and malignant cell lines and tissues. *Cancer Research*, 52, pp.3396-3401.

Xia, Y., Tang, G., Wang, C., Zhong, J., Chen, Y., Hua, L., Li, Y., Liu, H. and Zhu, B. 2020. Functionalized selenium nanoparticles for targeted siRNA delivery silence Derlin1 and promote antitumor efficacy against cervical cancer. *Drug Delivery*, 27, pp.15-25.

Xia, Y., Xiao, M., Zhao, M., Xu, T., Guo, M., Wang, C., Li, Y., Zhu, B. and Liu, H. 2020. Doxorubicin-loaded functionalized selenium nanoparticles for enhanced antitumor efficacy in cervical carcinoma therapy. *Materials Science and Engineering: C*, 106, p.110100.

Xia, Y., Xu, T., Wang, C., Li, Y., Lin, Z., Zhao, M. and Zhu, B. 2018. Novel functionalized nanoparticles for tumor-targeting co-delivery of doxorubicin and siRNA to enhance cancer therapy. *International Journal of Nanomedicine*, 13, p.143.

Xiao, K., Li, Y., Luo, J., Lee, J. S., Xiao, W., Gonik, A. M., Agarwal, R. G. and Lam, K. S. 2011. The effect of surface charge on *in vivo* biodistribution of PEG-oligocholic acid based micellar nanoparticles. *Biomaterials*, 32, pp.3435-3446.

Xu, J., Xu, B., Shou, D., Xia, X. and Hu, Y., 2015. Preparation and evaluation of vancomycin-loaded N-trimethyl chitosan nanoparticles. *Polymers*, 7, pp.1850-1870.

Yang, Y., Hou, J., Wang, P., Wang, C., Miao, L., Ao, Y., Wang, X., Lv, B., You, G. and Liu, Z. 2018. The effects of extracellular polymeric substances on magnetic iron oxide nanoparticles stability and the removal of microcystin-LR in aqueous environments. *Ecotoxicology and Environmental Safety*, 148, pp.89-96.

Yu, A., Shi, H., Liu, H., Bao, Z., Dai, M., Lin, D., Lin, D., Xu, X., Li, X. and Wang, Y. 2020. Mucoadhesive dexamethasone-glycol chitosan nanoparticles for ophthalmic drug delivery. *International Journal of Pharmaceutics*, 575, p.118943.

Yu, B., Li, X., Zheng, W., Feng, Y., Wong, Y.-S. and Chen, T. 2014. pH-responsive cancer-targeted selenium nanoparticles: a transformable drug carrier with enhanced theranostic effects. *Journal of Materials Chemistry B*, 2, pp.5409-5418.

Yuan, Y.-G., Zhang, S., Hwang, J.-Y. and Kong, I.-K. 2018. Silver nanoparticles potentiates cytotoxicity and apoptotic potential of camptothecin in human cervical cancer cells. *Oxidative Medicine and Cellular Longevity*, 2018, pp.1-21.

Zaleska-Medynska, A. 2018. Metal oxide-based photocatalysis: fundamentals and prospects for application. In *Metal Oxide Series,* Elsevier, 2018, pp.1-2.

Zeromski, J. 2002. Significance of tumor-cell receptors in human cancer. *Archivum Immunologiae et Therapiae Experimentalis,* 50, pp.105-110.

Zhang, H. and Toshima, N. 2013. Synthesis of Au/Pt bimetallic nanoparticles with a Pt-rich shell and their high catalytic activities for aerobic glucose oxidation. *Journal of Colloid and Interface Science*, 394, pp.166-176.

Zhou, L., Song, Z., Zhang, S., Li, Y., Xu, J. and Guo, Y. 2021. Construction and antitumor activity of selenium nanoparticles decorated with the polysaccharide extracted from *Citrus limon* (L.) Burm. f.(Rutaceae). *International Journal of Biological Macromolecules*, 188, pp.904-913.

Zohreh, N., Karimi, N., Hosseini, S.H., Istrate, C. and Busuioc, C. 2022. Fabrication of a magnetic nanocarrier for doxorubicin delivery based on hyperbranched polyglycerol and carboxymethyl cellulose: an investigation on the effect of borax cross-linker on pH-sensitivity. *International Journal of Biological Macromolecules*, 203, pp.80-92.

VII. Appendix

1. Synthesis and Characterization

1.1. UV- Spectroscopy

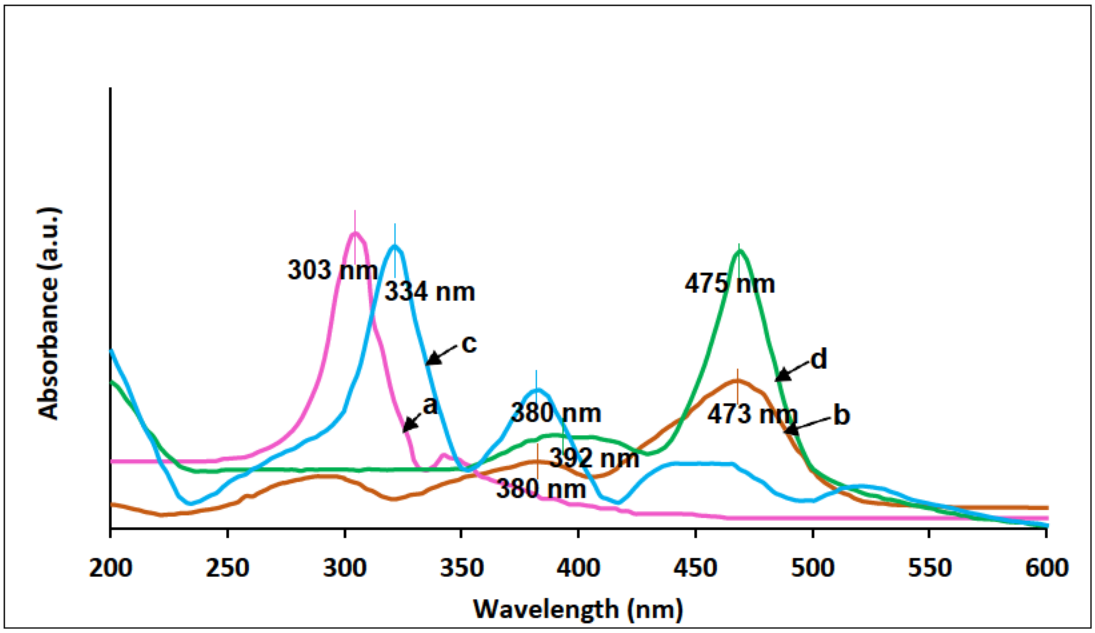

Figure A1: UV-vis spectra of (a)chitosan (Ch), (b) doxorubicin (DOX), (c) folic acid (FA), and (d) polyethylene glycol (PEG).

1.2. FTIR Spectroscopy

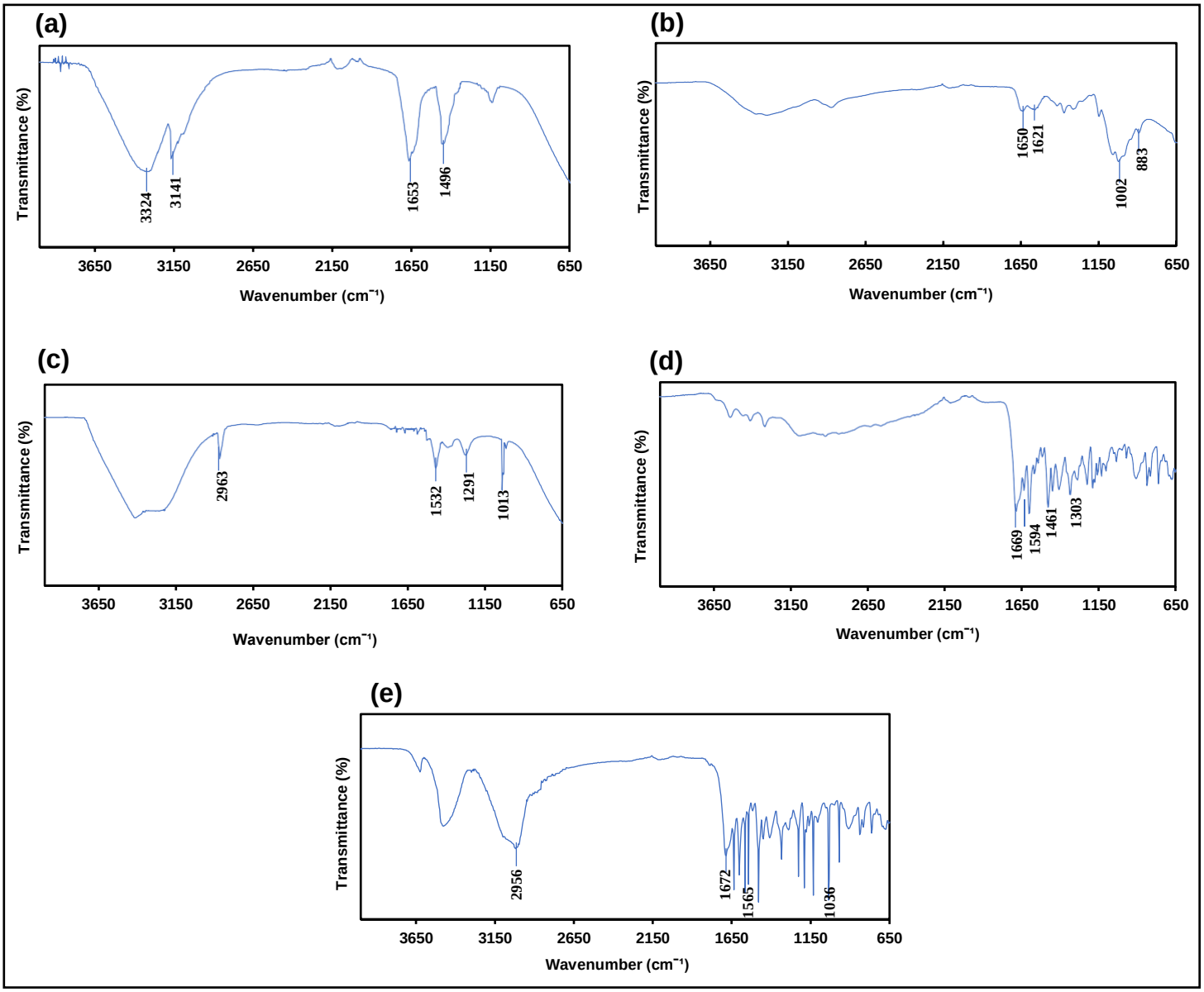

Figure A2 (a – e): FTIR spectra of (a) F-extract, (b) Ch, (c) PEG, (d) FA, and (e) DOX.

1.3. TEM, Size, and *Zeta* Potential

1.3.1. *Zeta* Potential

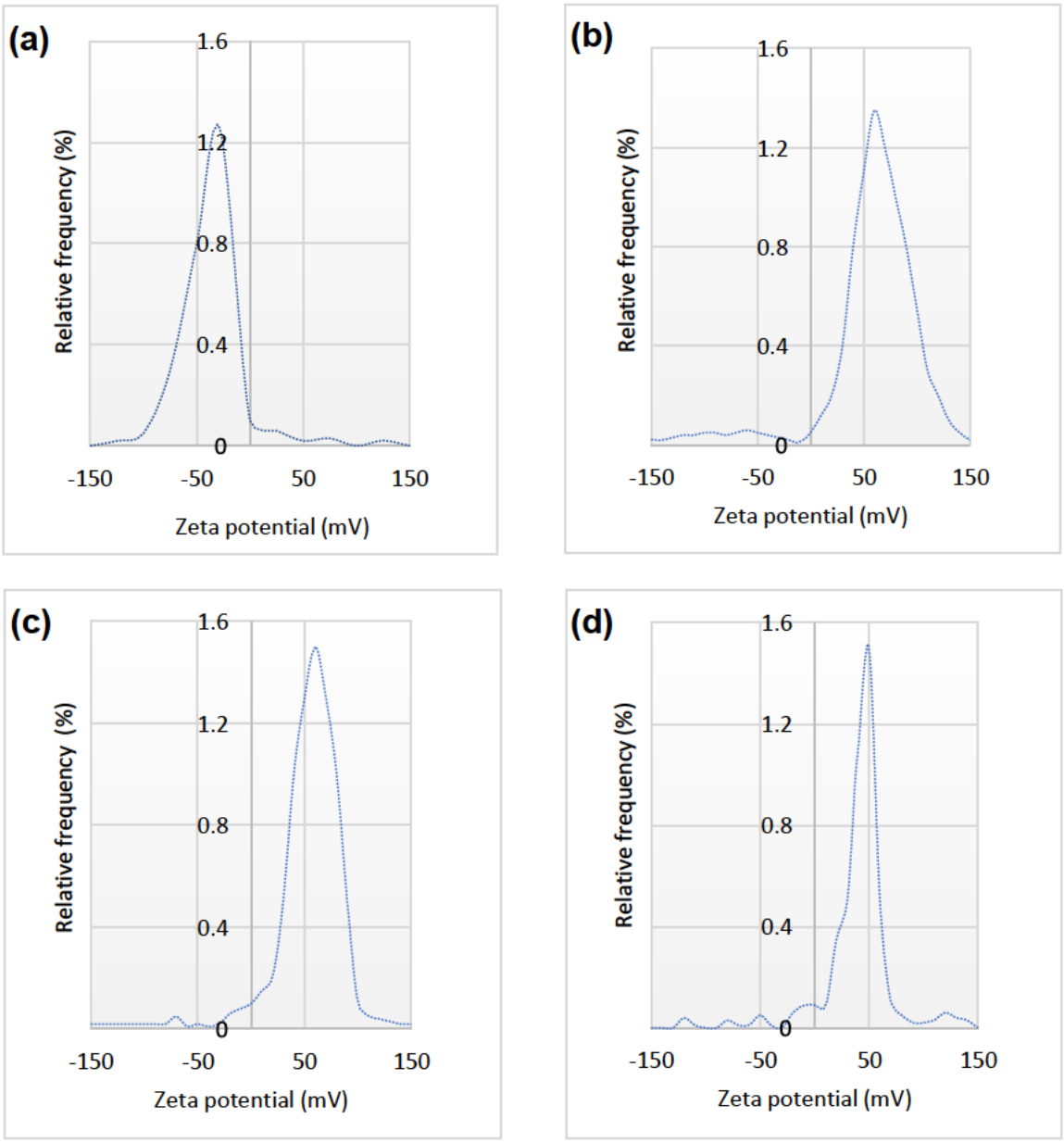

Figure A3 (a – d): *Zeta* potential of the chemically synthesized (a) SeAg NPs, (b) SeAgChPEG NPs, (c) SeAgChPEGFA NPs, and (d) SeAgChPEGFA@DOX NCs.

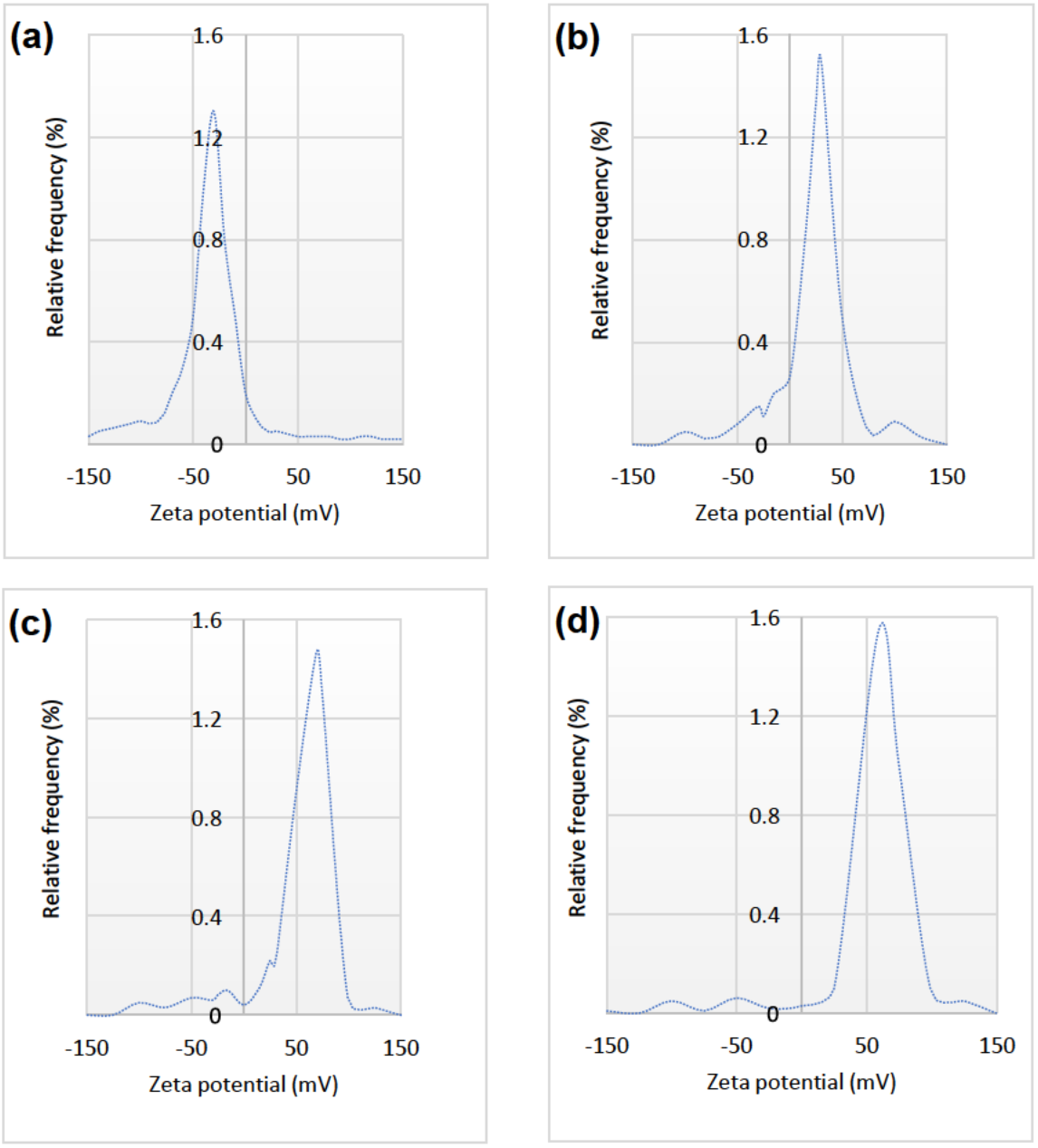

Figure A4 (a – d): *Zeta* potential of the biosynthesized (a) F-SeAg NPs, (b) F-SeAgChPEG NPs, (c) F-SeAgChPEGFA NPs, and (d) F-SeAgChPEGFA@DOX NCs.

2. Binding Studies

2.1. Drug Loading and Encapsulation Efficiency

Table A1: Drug loading and encapsulation efficiency percentages

Nanocomplexes (NCs)	Encapsulation efficiency (EE%)	Drug loading (DL%)
SeAgChPEGFA@DOX	84 ± 0.2	26 ± 2.1
F-SeAgChPEGFA@DOX	87 ± 0.4	22 ± 1.7

3. Cell Viability Studies

3.1. MTT Assay

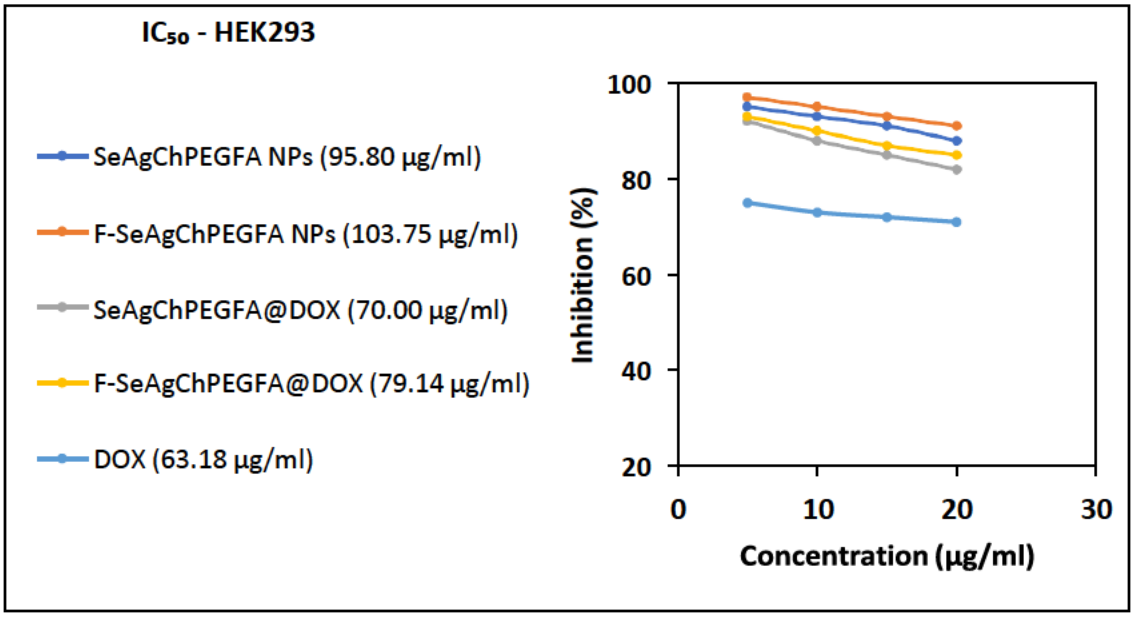

Figure A5: The half-maximal inhibitory concentration graphs of DOX-free NPs, their DOX-loaded NCs, and DOX on HEK293 cells.

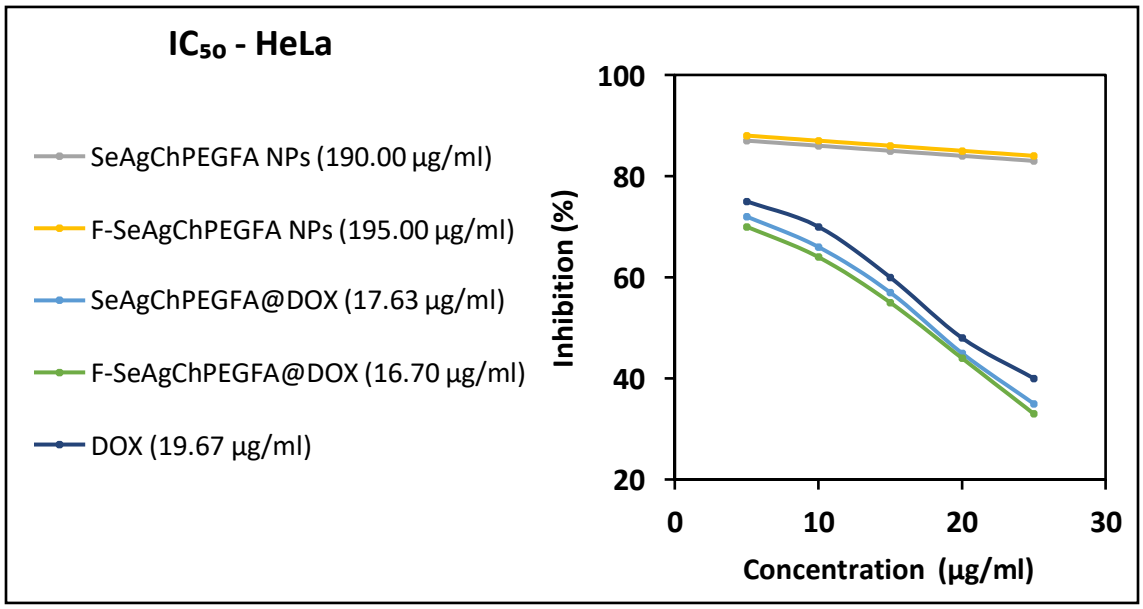

Figure A6: The half-maximal inhibitory concentration graphs of DOX-free NPs, their DOX-loaded NCs, and DOX on HeLa cells.